Check for updates

Zirconia-based nanomaterials: recent developments in synthesis and applications

Nisha Kumari,[a] Shweta Sareen,[b] Meenakshi Verma,[ac] Shelja Sharma,[a] Ajay Sharma,[ac] Harvinder Singh Sohal, [ID][a] S. K. Mehta, [ID][b] Jeongwon Park [ID] *[d] and Vishal Mutreja [ID] *[a]

In the last decade, the whole scientific community has witnessed great advances and progress in the various fields of nanoscience. Among the different nanomaterials, zirconia nanomaterials have found numerous applications as nanocatalysts, nanosensors, adsorbents, *etc.* Additionally, their exceptional biomedical applications in dentistry and drug delivery, and interesting biological properties, *viz.* anti-microbial, antioxidant, and anti-cancer activity, have further motivated the researchers to explore their physico-chemical properties using different synthetic pathways. With such an interest in zirconia-based nanomaterials, the present review focuses systematically on different synthesis approaches and their impact on the structure, size, shape, and morphology of these nanomaterials. Broadly, there are two approaches, *viz.*, chemical synthesis which includes hydrothermal, solvothermal, sol–gel, microwave, solution combustion, and co-precipitation methods, and a greener approach which employs bacteria, fungus, and plant parts for the preparation of zirconia nanoparticles. In this review article, the aforementioned methods have been critically analyzed for obtaining specific phases and shapes. The review also incorporates a detailed survey of the applications of zirconia-based nanomaterials. Furthermore, the influence of specific phases, morphology, and the comparison with their counterpart composites for different applications have also been included. Finally, the concluding remarks, prospects and possible scope are given in the last section.

[a]Department of Chemistry, University Institute of Science, Chandigarh University, Mohali, Punjab-140 413, India. E-mail: vishal.mutreja@gmail.com

[b]Department of Chemistry, Centre of Advanced Studies in Chemistry, Panjab University, Chandigarh-160 014, India

[c]Department of UCRD, Chandigarh University, Gharuan, Mohali, Punjab-140 413, India

[d]Department of Electrical and Biomedical Engineering, University of Nevada, Reno, NV 89557, USA. E-mail: jepark@unr.edu

Ms Nisha Kumari earned her B.Sc. (2006–2009) and M.Sc. (2009–2011) in Chemistry from Magadh University, Bodh Gaya, Bihar, India. Currently, she is pursuing a Ph.D. in Chemistry from Chandigarh University, Gharuan-Mohali.
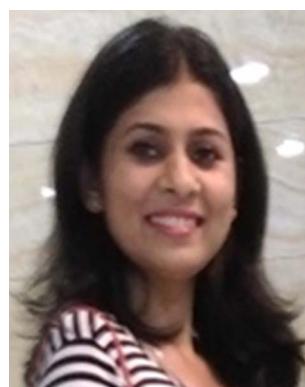
Shweta Sareen earned her B.Sc. and M.Sc. from Kurukshetra University, India. She obtained her Ph.D. in Chemistry from the Thapar Institute of Engineering & Technology, Patiala, in 2016. During her doctoral studies, she developed expertise in the design and synthesis of meso-porous silica-based nano-materials. She worked as a National Post-Doctoral Fellow at Panjab University, India from 2017 to 2019 on developing eco-friendly synthetic routes for mes-oporous silica materials for wastewater treatment. Currently, she is working as an Assistant Professor in the Department of Chem-istry at MCM DAV College, Chandigarh, India.

1 Introduction

Zirconium is a tough transition metal which has found boundless applications when present in its oxide form, known as zirconia or zirconium oxide. Zirconia is also known as ceramic steel owing to its intrinsic hardness, abrasiveness, high melting point, and low frictional resistance. In the nanoscale, it becomes immensely valuable owing to its high thermal stability, luminescence, refractive index, chemical stability, high specific area, biocompatibility, and exhibiting significant antibacterial, antioxidant, and antifungal properties. Such outstanding characteristics have motivated the scientific

Dr Meenakshi Verma obtained her Ph.D. degree from Thapar University, Patiala. She completed a National Post-doctoral fellowship from the Indian Institute of Technology, Ropar (IIT Ropar), and WIS-TEMM Fellowship from the University of Wisconsin, Green Bay, USA. Currently, she is working as an Assistant Professor at the University Centre for Research and Development, Chandigarh University, Punjab, India.

Dr Jeongwon Park joined the Department of Electrical and Biomedical Engineering at the University of Nevada, Reno, USA as an Associate Professor in July 2019. Prior to that, he was an Associate Professor at the School of Electrical Engineering and Computer Science at the University of Ottawa, Canada (2016–2021), and a scientist at SLAC National Accelerator Laboratory, Stanford University, USA (2014–2016). For six years (2008–2014), he served as a senior technologist to support the corporate chief technology officer (CTO) and business units at Applied Materials, USA. He has been a guest researcher at the Lawrence Berkeley National Laboratories (2005–2008), an adjunct professor in the Department of Electrical Engineering at Santa Clara University (2009–2016), and a visiting scholar in the Department of Electrical Engineering at Stanford University, CA, USA (2013–2014).

Dr S. K. Mehta, Fellow of Royal Society of Chemistry (FRSC) is Vice Chancellor, University of Ladakh, UT and Professor at the Department of Chemistry, Ex-Chairman, Chemistry and Ex-Director SAIF/CIL/UCIM, Panjab University, Chandigarh. He is among the world's top 2% scientists declared by Stanford University in 2021. He is highly active in significant areas of research such as metal-losurfactant chemistry, nano-electrochemical sensors, synthesis and application of semiconducting nanoparticles, colloidal chemistry, and nano-drug delivery systems. He has more than 402 publications in international journals of repute with an h-index of 59, citation index 10874, and i10 244, and is an author of about 25 books/chapters. He is a recipient of the renowned DAAD and JSPS fellowships, bronze medal from the Chemical Research Society of India (CRSI), Authors award by the Royal Society of Chemistry (UK), Haryana Vigyan Ratna award, Prof. W. U. Malik Memorial Award of the Indian Council of Chemists (ICC) and STE award. He has been a visiting scientist in the UK, Germany, Japan, USA, and France and has guided 15 post-doctoral, 49 Ph.D., and 50 masters students, and handled 20 research projects.

Dr Vishal Mutreja acquired his Ph.D. in 2014 from Thapar Institute of Engineering & Technology, formerly known as Thapar University, Patiala. The title of his Ph.D. thesis is "Development of Heterogeneous Catalysts for the Formation of Biodiesel". After completing his Ph.D., he served as Assistant Professor at Maharishi Markandeshwar University, Mullana-Ambala, India for 3 years (2014–2017). In 2017, he worked as a National Post-Doctoral Fellow (N-PDF) in the area of sensors at the lab of Prof. S. K. Mehta, Punjab University, Chandigarh, India. In 2019, he moved to Prof. Park's lab at the University of Ottawa, Canada as a Shastri-Indo Canadian post-doctoral fellow, where he gained expertise in the area of device fabrication. Currently, he is working as an Associate Professor at Chandigarh University, Mohali, Punjab-140 413, India.

community to explore zirconia-based nanomaterials in a wide range of technological fields such as functional materials, *viz.*, catalysts,[1] sensors[2] and semiconductor devices,[3] and structural materials, *viz.*, coating on cutting tools, ceramics,[4] implants,[5] *etc.* Apart from that, it can also be employed as a dielectric, electro-optic, and piezoelectric material due to its favourable optical and electrical properties.

Zirconia exists in three crystal phases, cubic, tetragonal, and monoclinic, in a typical air atmosphere and at distinct temperature ranges. The pure monoclinic phase is stable up to 1100 °C, the tetragonal phase is stable in the range of 1100–2370 °C and the cubic phase exists at temperatures over 2370 °C.[6] Among the different phases, the cubic and tetragonal crystals are found to be unstable in bulk forms at ambient temperature. Therefore, considerable efforts have been dedicated to stabilizing the unstable cubic and tetragonal crystal phases by doping with several divalent or trivalent cationic stabilizers such as Ca^{2+}, Mg^{2+}, Sc^{3+}, and Y^{3+} or by the reduction of particle/grain size to the nanometre scale.[7–10] Moreover, the interconversion of phases such as cubic to tetragonal and subsequently tetragonal to monoclinic takes place at higher temperatures and also affects the volume of zirconia nanomaterials significantly which ultimately limits their applicability in different fields such as catalysis, coatings *etc.* Another limitation of zirconia nanoparticles has been their tendency to undergo agglomeration during their synthesis. Furthermore, limited methods have been reported for the synthesis of anisotropic zirconia nanoparticles with the desired size range. In this regard, it appears quite worthwhile to critically analyze the various methods, routes, and reaction conditions for the synthesis of such versatile nanomaterials. Therefore, the present review article contributes toward a comprehensive analysis of the state-of-art specific synthetic methods for the preparation of zirconia nanomaterials for the desired applications and provides a database for novel future research perspectives. There are two major sections in this review paper; the first section involves details about different synthesis methods of zirconia-based nanomaterials and a critical analysis of the effect of various reaction parameters and methods on size, shape, and morphology, and in the second part, a variety of applications of these materials have been included. Finally, perspectives and scope of further developments of such materials have been given.

1.1 Synthesis of zirconia nanomaterials

The research interest in synthesizing ZrO_2 nanoparticles by various methods has increased considerably in the last decade owing to their diverse applications. There have been interesting findings in terms of shape, size, morphology, yield, and purity when different methods were employed. Broadly, there are two approaches: the chemical method and greener synthesis which are discussed below:

1.1.1 Chemical methods. Zirconia nanoparticles are prepared by different chemical methods to obtain the desired shape and size, and crystallinity. Various chemical methods for the synthesis of zirconia-based nanomaterials include

microwave-assisted approach,[11] hydrothermal,[12] sol–gel,[13] co-precipitation,[14] and solution combustion method. A wide variety of zirconia precursors such as $ZrOCl_2$, $ZrCl_4$, and $Zr(C_5H_7O_2)_4$, and different reagents have been employed in these methods for the synthesis of nanomaterials of different shapes and sizes. Various reaction parameters such as zirconia salts, pH, reaction time, and temperature can also influence the morphology and size range of nanoparticles. The effect of different chemical synthesis methods and reaction conditions on the morphology and size range of ZrO_2 is given in Table 1. The comprehensive details of the chemical methods are given below.

(i) Microwave-assisted approach. Microwave-assisted approaches are quite popular as they are facile, advantageous, rapid, and energy efficient and hence, have been extensively employed in nanomaterial synthesis. In addition, microwave heating proves to be beneficial over conventional heating approaches in a way that microwaves could achieve elevated temperatures quickly in a pressure-controlled environment and exhibit a tendency to attain optimum crystallinity. The microwave technique depends on the effective heating of matter by microwave dielectric heating which is the capacity of a solvent and reagent to retain microwave energy and to convert it into heat. In this technique, heating is generally accomplished through dipolar polarization and ionic conduction.[15] Different zirconia salts, *viz.* nitrate, sulphate, chloride, and chelating agents have been employed in this method. Singh and Nakate[16] reported the synthesis of zirconia nanoparticles by using the microwave method at a low temperature (80 °C) and studied their photoluminescence (PL) properties. Powder X-ray diffraction analysis revealed the formation of combined phases of monoclinic and tetragonal ZrO_2. The microscopic analysis confirmed that the sizes of nanoparticles were less than 10 nm. The specific surface area of ZrO_2 NPs was found to be 65.85 m^2 g^{-1}. These particles exhibited excellent optical properties such as an optical band gap of 2.49 eV and an intense emission peak at 414 nm in the photoluminescence spectrum.

Recently, Yousaf *et al.*[17] demonstrated the microwave synthesis of zirconia nanoparticles by using honey as a capping agent, for optical applications. The bandgap of the prepared tetragonal zirconia was found to be in the range of 4.7–4.82 eV. The structural characterization revealed the formation of single-phase tetragonal zirconium oxide with high purity under optimized conditions.

Similarly, Bukhari *et al.*[18] prepared zirconia nanofibers by a microwave-assisted sol–gel approach. In this study, honey was used as a structure-directing and capping agent to enhance the stability, reduce the crystallite size of nanofibers, and prevent the hard agglomeration of nanoparticles. Consequently, soft or less agglomeration resulted in a stabilized tetragonal phase of zirconia by inhibiting its interphase transformation from tetragonal into monoclinic (Fig. 1).

The microwave wattage (100–900 W) also significantly affected the stabilization of zirconia nanoparticles. Powder X-ray diffraction study revealed the formation of highly pure tetragonal zirconia at low microwave power ∼100 W with a smaller crystallite size of approximately 26 nm due to the

Table 1 Effect of different chemical synthesis methods and reaction conditions on the shape, size, and crystal structure of ZrO$_2$ NPs[a]

Chemical method	Materials	Solvent	pH	Reaction temperature/power and time	Thermal treatment	Crystal system, shape, size range, average size	Ref.
Microwave-assisted method	Zirconium oxychloride octahydrate, sodium hydroxide	—	—	80 °C, 12 min	400 °C, 2 h	Mixed phase (monoclinic and tetragonal), spherical (8–10) nm, 8.8 nm, –	41
	Zirconium oxychloride, anhydrous citric acid	—	2	–, 2 min	450 °C, 4 h	Tetragonal, –, –, ~5–10 nm	42
	Zirconium oxychloride, sodium hydroxide	—	12	–, 6 min	600 °C, 4 h	Monoclinic, –, 32–38 nm, –	43
	Zirconyl nitrate monohydrate, L-serine amino acid	Water	—	800 W, 60 s	400 °C, 600 °C, 800 °C, –	Cubic, –, –, 70, 76 and 77 nm	44
	Zirconium oxychloride octahydrate	Water	—	100–1000 W, –	–, –	Tetragonal, –, –, –	19
	Zirconium oxychloride octahydrate, honey	Water	—	~100 W, –	–, –	Tetragonal, –, –, ~26 nm	18
	Zirconyl oxynitrate	1,4-Butanediol	—	800 W, 10 min	–, –	Tetragonal, –, –, ~10 nm	20
Hydrothermal method	ZrO(NO$_3$)$_2$·xH$_2$O, sodium hydroxide	—	—	150 °C, 4 h	110 °C, 90 min	Monoclinic, –, ~25 nm	23
	Zirconyl chloride octahydrate, glucose monohydrate	Water	—	180 °C, 20 h	550 °C, 4 h	–, sphere, ~8 nm, –	26
	Commercial zirconia, sodium hydroxide	—	—	150 °C, 85 h	–, –	Mixed phases (monoclinic, tetragonal and cubic), –, –, 15–30 nm	12
	Zirconium oxychloride, sodium hydroxide	Ethanol and water	14	–, –	400 °C and 500 °C, 2 h and 0.5 h	Tetragonal, –, 2–11 and 3–12 nm, 4.5 and 6 nm	21
	Zirconyl nitrate, CTAB/SDS/triton, ammonium hydroxide	—	12	90 °C, 12 h	500 °C, 2 h	–, varied, varied, –	27
Sol–gel	Zirconium(IV) propoxide, acetic acid, nitric acid	Isopropanol	2.5	–, –	700 °C, 1 h	Monoclinic, –, 25.39 nm, –	32
	Zirconium(IV) propoxide, nitric acid	—	—	–, 1 h	500 °C, 2 h	Tetragonal, –, –, 30–60 nm	33
	Zirconium n-propoxide, glucose, fructose, aqueous ammonia	—	9–10	RT, 1 h	700 °C, 3 h	Tetragonal and monoclinic, –, 10–30 nm, –	13
	Zr(SO$_4$)$_2$·H$_2$O, sodium lauryl sulfate	Benzyl alcohol	—	—	600 °C, 5 h	Tetragonal and monoclinic, –, 9.7 nm, –	45
	Zr(acac)$_4$, sucrose	Ethanol	~12	110 °C, 10 min	300–650 °C, –	Tetragonal and monoclinic, –, –, –	35
Co-precipitation	Zirconium nitrate hexahydrate, potassium hydroxide	Water	>10	RT, –	900 °C, 4 h	–, spherical (193 nm), –, –	38
	Zirconyl chloride octahydrate, diammonium oxalate monohydrate, ethylene glycol	Water	—	Varied, varied	Varied, varied	Monoclinic, spherical, –, 12.85 nm	39
	Zirconium(IV) nitrate, tetraethyl ortho-silicate, ammonium hydroxide	Water and ethanol	7	348 K, 10 min	1173 K, 10 min	Tetragonal, –, 3.3 nm, –	40

[a] RT: room temperature.
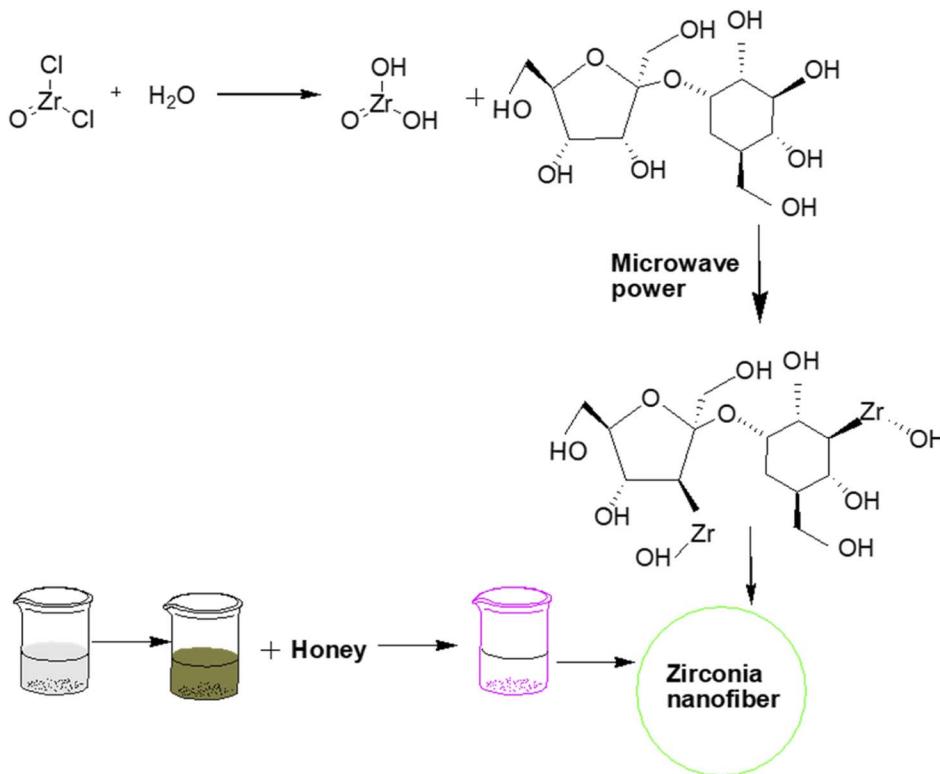
Fig. 1 Honey mediated microwave assisted sol–gel synthesis of stabilized zirconia nanofibers.[18]

presence of an optimum quantity of honey to coat the zirconia particles.

In another interesting report by Batool *et al.*,[19] the preparation of zirconia nanoparticles and the dilemma of long-term stability were addressed. The obtained tetragonal zirconia nanoparticles were found to be stable even after a period of 6 to 12 months at room temperature.

Recently, Mishra *et al.*[20] demonstrated the synthesis of tetragonal zirconia nanoparticles having an average crystal size of 10 nm using a microwave-assisted solvothermal route. In this study, the bandgap of the prepared nanoparticles was found to be 3.67 eV.

(ii) Hydrothermal and solvothermal approach. The hydrothermal method is a promising approach for synthesizing nanomaterials and involves heating the mixture of precursors, appropriate agents (reducing, oxidizing, hydrolyzing), and suitable solvent in a closed vessel which facilitates the fabrication of nanocrystals with controlled surface alteration, morphology, size, and stability. Apart from that, such kinds of synthesis methods are also useful for doping heteroatoms in nanoparticles or fabrication of nanocomposites owing to the generation of high pressure in a closed vessel. These methods have been used for the preparation of zirconia nanoparticles as well as for the doping of zirconia with foreign species. For instance, Behbahani *et al.*[12] reported the hydrothermal synthesis of zirconia nanoparticles by using commercial monoclinic zirconia in an alkaline medium. Some of the parameters such as the concentration of the initial solution and

pH were varied accordingly to obtain novel nanoparticles with desired shape and size. All three phases of zirconia, *viz.*, cubic, tetragonal, and monoclinic phases, were observed and the corresponding sizes were found to be in the range of 15–30 nm.

Usually, attempting the synthesis of t-ZrO$_2$ nanoparticles by using an inorganic precursor without any surfactant results in the agglomeration of particles. Under such circumstances, the hydrothermal corrosion method, which involves a corroding medium such as H$_2$SO$_4$, HCl *etc.* to break down hard aggregates into dispersed fine nanoparticles during the hydrothermal treatment, could be employed. Zhou *et al.*[21] demonstrated the hydrothermal–corrosion method to produce highly dispersed tetragonal zirconia nanoparticles (less than 10 nm) without using any surfactants. It was stated that the dispersity and crystallinity of the prepared tetragonal ZrO$_2$ powders can be modified by using reaction conditions such as calcination of the precipitates followed by hydrothermal HCl corrosion at different temperatures. In the follow-up study, Sagadevan *et al.*[22] investigated the synthesis of spherical zirconia nanoparticles by the hydrothermal technique. The optical band gap of 5.02 eV and photoluminescence measurements confirmed the presence of oxygen vacancies accompanied by intrinsic defects in such NPs.

Ahmad *et al.*[23] successfully prepared ZrO$_2$ nanoparticles in an alkaline medium by employing the hydrothermal technique. Investigation of the structure and phase composition of the ZrO$_2$ nanoparticles by powder X-ray diffraction indicated the presence of pure monoclinic zirconia. The dielectric investigations suggested that ZrO$_2$ nanoparticles could be used for

storage and electronic devices owing to the values of dielectric constant and dielectric loss, which were 7.5 and 0.0094, respectively.

Meetei et al.[24] demonstrated the synthesis of white light-emitting nanocrystals composed of cubic ZrO_2 doped with Eu^{3+} via the hydrothermal method. In this study, the dopant Eu^{3+} was employed to stabilize the cubic phase with simultaneous production of the red counterpart from the white light. The wide range of photoluminescence emission arose due to the oxygen vacancies which could coalesce with a dopant to produce white light within the sample. The prolonged lifetime of the red counterpart of the sample could efficiently rectify the issue of the brief lifetime of traditional phosphors. Such materials could be beneficial in simulating the daylight of the sun by preparing light-emitting diodes, electronic flash, and lights for theatres and operas.

Noh et al.[25] showcased the synthesis of anisotropic-shaped zirconia nanocrystals by using amorphous zirconium hydroxide powder and tetragonal zirconia powder at 150–250 °C along with varying concentrations of sodium hydroxide as an additive. The higher temperature facilitated the transformation of nanocrystals from spherical into spindle/rod-like structures with increase in the monoclinic phase fraction. Additionally, the fraction of the monoclinic phase was also found to increase with increasing sodium hydroxide concentration.

Abdelaal et al.[26] reported a one-pot method for the fabrication of hollow sub-microspheres of zirconia having a diameter of 300 nm and a wall of thickness of 8 nm. In the first step, in situ preparation of the core@shell composite was achieved via autoclaving of glucose monohydrate as a core and sacrificial template, and zirconyl chloride octahydrate as the oxide precursor. Subsequently, calcination at 550 °C for 4 h resulted in the formation of a hollow sphere of ZrO_2 due to the removal of the template.

In another study, Nath et al.[27] reported the synthesis of highly thermally stable zirconia nanoparticles by a surfactant-assisted hydrothermal route (Fig. 2). Different types of surfactants such as cetyltrimethylammonium bromide (CTAB), sodium dodecyl sulfate (SDS), and Triton X-100 were used in the synthesis. Consequently, different morphologies of nanocrystals, for example, rod and mortar–pestle-shaped particles with different sizes were obtained. The distinct modifications in phase composition and morphology can also be achieved by tuning the reaction conditions during the preparation of the nanoparticles.

Stolzenberg et al.[28] demonstrated the fractal growth of ZrO_2 nanocrystals by varying the temperature and concentrations of the zirconia precursor and benzyl alcohol during their synthesis. A possible reaction mechanism for the non-aqueous preparation of ZrO_2 NPs under solvothermal conditions was proposed. The growth mechanism involved two steps, in the first step, the precursor reacted with benzyl alcohol (solvent) through a ligand exchange to convert it into an intermediate which finally reacts in a subsequent ether condensation reaction to form zirconia nanoparticles (Fig. 3). During the growth of NPs, the size increases from 2.7 nm to 7 nm along with phase transformation from tetragonal into monoclinic. Transmission electron microscopic images revealed that the nanoparticles grew from a round shape to a dendritic form along with the transformation of phase. In contrast to the supposition that only thermodynamics could control phase transformation, the reported study proposed that phase transition could be controlled by kinetics as well.

Zirconia nanotubes in the range of 60–90 nm were also prepared by hydrothermal treatment. For this, 50 mL aqueous solution of each of $ZrO(NO_3)_2 \cdot xH_2O$ (0.5 M) and NaOH (5 M) were uniformly mixed followed by the addition of 2 mL of absolute ethanol as a buffering agent. The final mixture was taken in a hydrothermal vessel which was heated at 250 °C for 14 h.[29]

Shu et al.[30] also demonstrated the synthesis of unique star-shaped particles in the range of 40–100 nm having a tetragonal phase via hydrothermal treatment. For this, $ZrOCl_2$ and sodium acetate were dissolved in water in a 1 : 2 molar ratio and subjected to hydrothermal treatment at 240 °C for 6 h. Subsequently, the product was separated via centrifugation and dried at 90 °C.

Reddy et al.[31] demonstrated that hydrothermal treatment of a zirconyl chloride octahydrate precursor and NH_4OH at 200 °C for 12 h could result in pure tetragonal zirconia NPs without using any template. The prepared nanoparticles were spherical.

(iii) Sol–gel approach. The sol–gel method involves the formation of a sol which is a colloidal solution of solid particles, followed by the formation of a gel which is an interconnected network of polymerized particles in a separate phase (solvent). Zirconia nanoparticles could also be prepared by the sol–gel

$$ZrO(NO_3)_2 + CTAB \xrightarrow[\text{90°C/12 hr.}]{NH_4OH} Zr(OH)_2 \cdot CTAB \text{ Complex} + ZrO((OH)(NO_3)^- \text{ CTAB Complex} + NH_4NO_3$$

Calcination/500°C

Mesoporous nanocrystalline ZrO_2
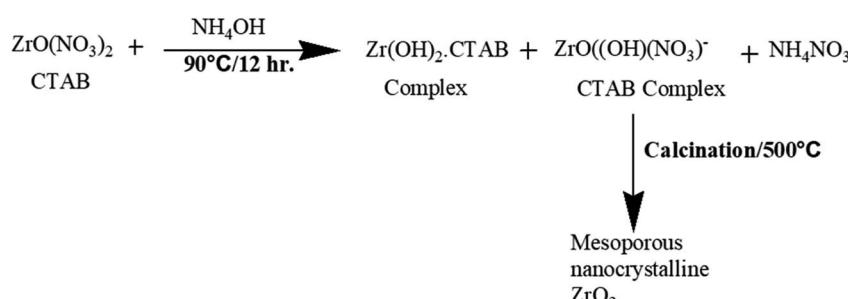
Fig. 2 Formation mechanism of mesoporous nanocrystalline zirconia.[27]
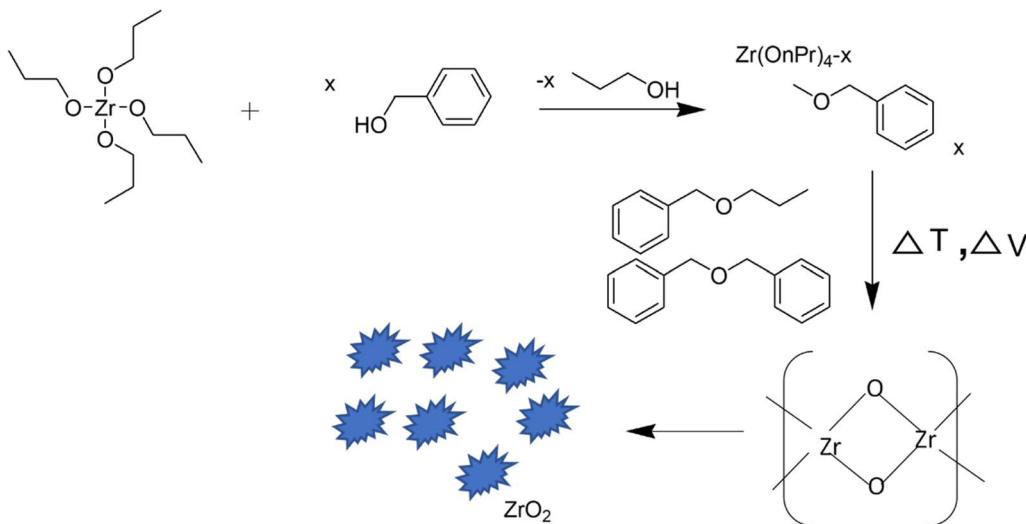
Fig. 3 Reaction mechanism of the nonaqueous synthesis of ZrO_2 nanoparticles.[28]

method wherein, the sol can be obtained by dissolving a metal alkoxide or an organo-metallic precursor in water or alcohol which, under suitable reaction conditions (temperature, aging time, *etc.*), undergoes phase transformation into a gel-like structure. In the gel, owing to the network structure, polymeric particles remain separated, therefore the sizes of the particles can be controlled and agglomeration can be prevented. Finally, the gel upon suitable heat treatment could lead to the formation of nanoparticles. The principal advantage of the sol–gel method is the formation of uniform nanostructures at comparatively low temperatures as can be seen in Table 1. In this method, the reactivity of the precursors can be modified by alteration with chelation agents, consequently the gelation process could also be influenced, and ultimately the size and shape of the particles can also be modified. The different chelating reagents that have been employed for the preparation of nano zirconia are acetylacetone, acetic acid, citric acid, and different sugars (*e.g.*, sucrose, maltose, glucose).

Madhusudhana *et al.*[32] reported the synthesis of monoclinic zirconia nanoparticles by a facile sol–gel technique using acetic acid as a chelating agent. The resultant nanoparticles were found to be suitable for thermal applications due to their high resistance behavior to crack propagation. Lim *et al.*[33] developed a synthesis of tetragonal phase zirconia nanoparticles. Different concentrations of NH_3 solution and nitric acid were used with zirconium isopropoxide to analyze the impact on the crystallinity and particle size of ZrO_2. In contrast, smaller sizes of nanoparticles were obtained when nitric acid was used instead of ammonia in the reaction mixture.

Bahari *et al.*[34] investigated the preparation of ZrO_2 at a relatively lower temperature. It was observed that some amount of the monoclinic phase gets converted into metastable tetragonal ZrO_2 during heating. Heshmatpour *et al.*[13] reported a simple sol–gel synthesis of zirconia nanoparticles of uniform size. Glucose and fructose were used as organic additives which could prevent the phase transition from the monoclinic to the tetragonal phase.

Likewise, the synthesis of zirconia thin films having a pure tetragonal phase was reported by Majedi *et al.*[35] *via* a sucrose-mediated sol–gel method. Initially, for preparing the sol, the zirconium(IV) acetylacetonate precursor was stirred in ethanol at 70 °C for 30 min followed by the addition of an ammoniacal solution as the hydrolyzing agent. Subsequently, sucrose was added to the solution as a gelation agent under stirring at 110 °C which results in the formation of the sol. The as-obtained sol was transformed into a xerogel by drying in an oven at 80 °C for 24 h. Furthermore, calcination at 350–500 °C results in t-zirconia, and calcination at 650 °C results in the formation of a mixture of the tetragonal and monoclinic phases. Such findings were expected as the post-calcination temperature could influence phase formation as well as phase transition.

Sponchia *et al.*[36] demonstrated a simple and efficient neutral surfactant-assisted sol–gel method for the synthesis of spherical mesoporous zirconia nanoparticles by using a zirconium propoxide precursor, surfactant, ethanol, and alkali halide, followed by solvothermal thermal treatment using ethanol and water. The obtained dried powder was subjected to heat treatment under vacuum conditions to extract the surfactant without any structural modification. The prepared material exhibited a high surface area in comparison to literature reports. The effect of the addition of different alkali halides on the shape and size of the nanoparticle was also investigated. The salt's solubility plays a crucial role in governing the particle size. Biological experiments demonstrated that mesoporous zirconia nanoparticles were biocompatible, degradable, and cell-permeable, therefore they could be employed for theranostic applications.

For instance, Davar *et al.*[37] synthesized pure monoclinic zirconia nanosheets by the polymeric sol–gel method. In this method, zirconium acetylacetonate was used as an organic metal precursor (Zr^{4+}), and citric acid and ethylene glycol were used as the source of chelation and polymerization agents respectively. By varying the molar ratio of ethylene glycol to citric acid in the synthesis procedure, the phase as well as

© 2022 The Author(s). Published by the Royal Society of Chemistry

morphology of the nanoparticles could be modified. With increase in mole ratio from 5 : 5 to 90 : 5, the phase changes from cubic to monoclinic, and morphology varies from semi-spherical to nanosheets.

(iv) Co-precipitation technique. Co-precipitation is an easy approach to prepare metal oxide nanoparticles using an aqueous solution of metal salts (chloride and nitrate metal salts) and bases such as ammonia or sodium hydroxide followed by heating or calcination at a suitable temperature. It involved nucleation followed by growth upon the addition of a precipitating agent; subsequently, heat treatment (calcination) led to the formation of metal oxide nanoparticles.

Ramachandran *et al.*[38] reported a co-precipitation method for the synthesis of zirconia nanoparticles using zirconium nitrate as the precursor and KOH as the precipitating agent. The ratio of zirconium nitrate and KOH (0.5, 1, and 1.5 M) was optimized to obtain crystalline zirconium oxide with spherical morphology. At the same line, Foo *et al.*[39] demonstrated the preparation of uniformly shaped zirconia nanoparticles having crystal sizes in the range of 6 to 35 nm. In this study, it was demonstrated that the calcination temperature in the reaction procedure could significantly impact the surface morphology, crystal size, and purity of the resulting ZrO_2 NPs. A higher calcination temperature increased the degree of agglomeration and size of crystals. Similarly, Huang *et al.*[40] also demonstrated that calcination temperature and time could drastically influence the crystallite size of tetragonal ZrO_2. In this study, when the freeze-dried precursor powder was calcined at 1173 K, crystallites of size 3.3 nm were obtained; however, comparatively bigger crystallites of 20 nm were observed upon calcination at 1473 K.

(v) Solution combustion method. The solution combustion method involves the propagation of self-sustained and coupled complex exothermic reactions in an aqueous solution which could result in the formation of a ZrO_2 powder along with emission of various gases such as N_2, CO, CO_2, *etc.* It starts with the burning/oxidation of a fuel which is an organic compound employed as a reactant along with a metal precursor. This method has been used in the synthesis of a variety of nanomaterials, including zirconia nanoparticles. Manjunatha *et al.*[44] synthesized the pure cubic phase of ZrO_2 mesoporous nanoparticles *via* a microwave-assisted combustion method. In this procedure, zirconyl nitrate monohydrate ($ZrO(NO_3)_2 \cdot H_2O$) was used as the metal precursor and L-serine amino acid was employed as the fuel. Both components were dissolved in a minimum quantity of de-ionized water. Subsequently, the excess water was allowed to evaporate to obtain a viscous gel which upon microwave irradiation at 800 W for 60 seconds led to vigorous boiling followed by dehydration. Subsequently, the material gets burnt leading to the liberation of gases such as CO_2, N_2, and water vapour, and the formation of a white ZrO_2 powder having a cubic phase. This study indicated that both the crystallinity and band gap (~5.21 eV) of the prepared nanoparticles increases with increase in calcination temperature. An increase in band gap was observed due to a decline in the number of intermediate energy levels owing to an increase in orderliness with a smaller number of defects. The

photoluminescence spectrum displayed an intense violet emission band peak centred at 387 nm, owing to the existence of oxygen vacancies in the zirconia matrix. The surface area analysis revealed that such nanomaterials were mesoporous in nature and the pore size also tends to decrease with an increase in the calcination temperature.

Dwivedi *et al.*[42] prepared ZrO_2 NPs by a microwave-driven citrate sol–gel technique. In this study, the prepared zirconia nanoparticles exhibited a smaller size due to gelation and rapid combustion.

Prakash Babu *et al.*[46] also introduced a simple low-temperature solution combustion method without any stabilizing agent and calcination. In this method, zirconyl nitrate as the metal precursor and oxlayl di-hydrazide as the fuel were dissolved in water. The aqueous solution was taken in a dish and subjected to heat treatment at 400 °C in a preheated muffle furnace. Zirconia nano-powder having a cubic phase and crystallite size in the range from 6 to 12 nm was obtained.

Similarly, Tang *et al.*[47] reported the synthesis of hollow mesoporous zirconia nanocapsules with a porous shell structure. In this study, first, monodispersed silica nanoparticles were prepared *via* Stober's method using concentrated ammonia, water, ethanol, and TEOS followed by the formation of the $SiO_2@ZrO_2$ composite using $Zr(OBu)_4$. Finally, the composite was treated with NaOH (5 M) to remove silica which resulted in the formation of hexagonal mesoporous ZrO_2.

Though different methods for the formation of specific phases have been reported, microwave-assisted sol–gel and solution combustion methods can be identified as promising choices for the formation of specific phases. Particularly, with the solution combustion method, formation of the cubic phase has been observed predominantly. This could be due to the attainment of high temperature that favors the formation of the cubic phase which is also a high-temperature stable form of zirconia. Interestingly, the use of microwave treatment in the case of the sol–gel has also resulted in the formation of selective phases, particularly the tetragonal phase. Apart from that, employing a corrosive solvent (HCl, H_2SO_4) during the hydrothermal treatment of zirconia nanoparticles could be a useful approach for obtaining monodisperse nanoparticles.

In most of the published literature studies on zirconia nanomaterials, the formation of spherical particles has been reported. However, in some studies, the formation of unique shapes has also been reported using unusual reaction conditions and precursors. For instance, the formation of nanosheets has been reported *via* the sol–gel method using zirconium acetylacetonate as the metal precursor, and the formation of cubic and star-like shapes has been reported *via* the hydrothermal method at a comparatively higher temperature of 240–250 °C.[29,30,48] Interestingly, comparatively smaller particle sizes have been observed along with the pure tetragonal phase in all types of chemical synthesis methods.

1.1.2 Greener methods. Nowadays greener pathways for the synthesis of nanoparticles are being explored as they could enhance their biocompatibility, reduce the cost of the designed nanomaterial, and take care of environmental concerns.[49] In this context, the incredible commitment of Paul and Richard
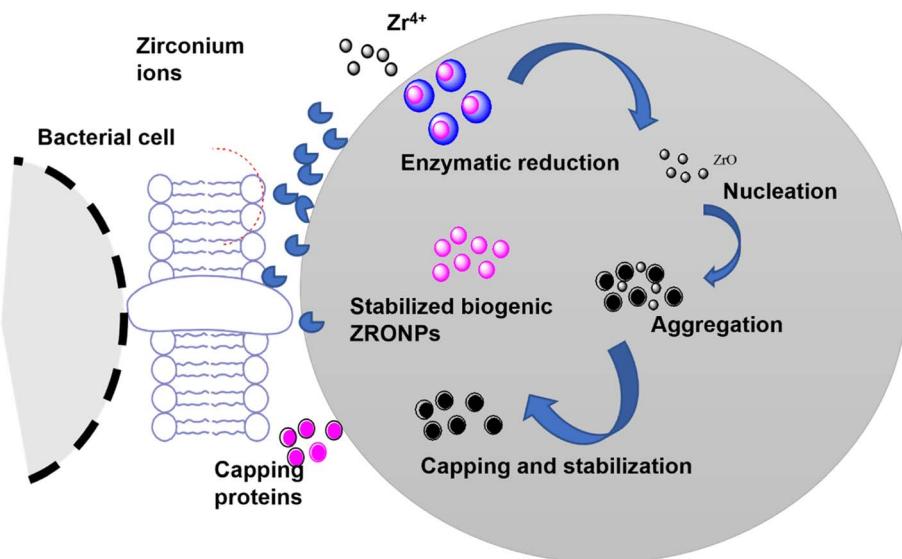
Fig. 4 Schematic representation of proposed extracellular biosynthesis mechanisms of ZrO$_2$ NPs. Nitrate reductase enzyme is responsible for the reduction of metal ions to their respective metal atoms that lead to nucleation and formation of NPs.[53]

toward making nanotechnology and green science doable is appreciated. Synthesis of metal nanoparticles using renewable and natural sources of reducing, stabilizing, and capping agents (microbes and parts of plants) is considered a greener approach. Microbial synthesis of nanoparticles includes microorganisms, such as bacteria, fungus, *etc.*, which could play a significant role in the reduction and stabilization of nanoparticles.[50,51] Nanoparticles can be synthesized *via* both intracellular and extracellular pathways. The intracellular pathway involves the transportation of metal ions into the cell by interaction with the negative receptors of the cell wall followed by the reduction of metallic species by the enzymes of the cell, whereas the extracellular synthesis of the nanoparticle is mediated by nitrate reductase which reduces the zirconium ions. Subsequently, the formation of nanoparticles takes place *via* nucleation, aggregation, and growth (Fig. 4).[52,53] Furthermore, stabilization of nanoparticles is known to occur due to capping agents (protein species) released by the cell wall. Uddin *et al.*[54] reported extracellular biosynthesis of ZrO$_2$ nanoparticles by using potassium hexafluorozirconate (K$_2$ZrF$_6$) as a precursor and the fungus *Humicola* sp. The characterization results revealed the presence of protein on the surface of quasi-spherical NPs. In the follow-up study, Bansal *et al.*[55] demonstrated the synthesis of zirconia nanoparticles *via* extra-cellular hydrolysis

of the metal halide precursor (ZrF$_6^{2-}$) by the cationic protein species (molecular weight 24 and 28 kDa) of the fungus *Fusarium oxysporum*. It involves the formation of a complex at room temperature under acidic conditions. Shanmugasundaram *et al.*[56] demonstrated a one-pot biosynthesis of non-toxic ZrO$_2$ nanoparticles (of size 44 ± 7 nm) using *Acinetobacter* sp. KCSI1 at room temperature. The zeta potential of the as-synthesized zirconia nanoparticles was found to be 36.5 ± 5.46 mV. Similarly, Ahmed *et al.*[53] demonstrated the synthesis of spherical-shaped zirconia nanoparticles (33–75 nm) by using *Enterobacter* sp. The key reaction parameters and important findings from such reports have been summarized in Table 2.

Nowadays, extracts of different parts of plants such as roots, leaves, flowers, and fruits are also being used for the preparation of nanomaterials. Various phytochemicals, *viz.* flavones, terpenoids, sugars, ketones, aldehydes, carboxylic acids, and amides, are found to be responsible for the reduction of metal precursors. These species act as both stabilizing and reducing agents. In general, the plant-mediated synthesis of zirconia NPs is a simple and facile process, in which a zirconia salt, such as zirconium oxychloride or zirconia nitrate is mixed and stirred with an appropriate plant extract at a suitable temperature followed by heat treatment. However, there are limited reports on the mechanism of formation and stabilization of zirconia

Table 2 Effect of different microorganisms and pH on the shape, size, and crystal structure of ZrO$_2$ NPs

Microorganism	Zirconia source	pH	Size range, average size (nm)	Crystal system, morphology	Ref.
Humicola sp. (fungus)	Potassium hexafluoro zirconate	9	13 nm	–, quasi-spherical	54
Fusarium oxysporum (fungus)	Potassium hexafluoro zirconate	3.6	7.3 ± 2.0 nm	Monoclinic, –	55
Acinetobacter sp. KCSI1 (bacteria)	Zirconium oxychloride octahydrate	2	44 ± 7 nm	—	56
Pseudomonas aeruginosa (bacteria)	Zirconium oxychloride octahydrate	—	6.41 nm	Monoclinic and tetragonal, –	66
Enterobacter sp. (bacteria)	Zirconium oxychloride octahydrate	—	33–75 nm	–, spherical	53

NPs from such biomolecules. Different reaction parameters, and resultantly different findings in terms of crystal structure and size distribution from recent reports on plant-mediated synthesis have been summarized in Table 3.

Silva et al.[57] demonstrated a green approach for the preparation of zirconia nanoparticles, exhibiting monoclinic and tetragonal phases by using Euclea natalensis plant extract. In this study, factorial design suggested that a higher concentration of precursor, lower amount of extract, and higher calcination temperature supported the synthesis of the tetragonal phase. Moreover, a possible mechanism (Fig. 5) for the preparation of ZrO_2 NPs using phytochemicals of Euclea natalensis such as pentacyclic terpenoids (lupeol, betulin, and β-sitosterol) and naphthoquinones (diospirine, shinanolone, and 7-methyl juglone) is also given in this report. However, there is ambiguity in the mechanism of formation of ZrO_2 NPs. It involves three steps: the reduction of zirconyl ions, the grouping of nanoparticles, and the growth of nanoparticles. But, only the reduction of zirconium ions could not lead to the formation of ZrO_2 as oxidation is also a necessary step for its formation. In another report,[58] bioreduction of zirconium ions, followed by complexation with water molecules, chelation with phytochemicals and finally oxidation were the major suggested steps in the plant-mediated synthesis of zirconia. As per our recent investigation on the plant-mediated synthesis of ZrO_2, which is in the process of publication, a change in the oxidation state of zirconium from +4 to +2 followed by complexation with phytocomponents was observed. The complex upon heat treatment regains its oxidation state of +4 in zirconia as that of the precursor ($ZrOCl_2$). These findings were supported by DFT calculations.

Another study on the green fabrication of ZrO_2NPs was reported by Jalill et al.[59] and the prepared nanoparticles exhibited excellent antifungal and antibacterial activity. Shanthi et al.[60] synthesized ZrO_2 nanoparticles by employing aqueous leaf extracts of Acalypha indica as a reducing agent. Encouraged by previous studies, Padma et al.[61] fabricated zirconium dioxide nanoparticles using Azadirachta indica leaves. Similarly, Sathish et al.[62] synthesized zirconia nanoparticles using Curcuma longa tuber. In this study, a higher pH was found to be favorable for the fabrication of zirconia NPs. Similarly, Gowri et al.[63] investigated the greener synthesis of spherical zirconia nanoparticles using Aloe vera plant extract. The nanoparticles were found to have sizes in the range of 50–100 nm. Majedi et al.[64] reported the synthesis of cubic phase zirconia nanoparticles using zirconium acetate as the precursor and lemon juice as the reducing agent. The impacts of sucrose addition on enhancing the particle size and the yield of the product were examined. A mixture of 20 mL lemon juice and sucrose was found to show a positive effect on uniform morphology having an average particle size of 21 nm. The as-prepared nanoparticles were employed in electrolyte materials for intermediate or low-temperature solid oxide fuel cells. Saraswathi et al.[65] demonstrated the fabrication of tetragonal zirconia nanoparticles (2 nm) using Lagerstroemia speciosa leaves. The authors investigated the photocatalytic activity of the nanoparticles by

Table 3 Effect of different reaction conditions and plant extract on the shape, size, and crystal structure of ZrO₂ NPs

Plant	Zirconia source	Conc. of plant extract, precursor, ratio	Reaction temperature, time	Thermal treatment (drying and calcination)	Size range, average size (nm)	Crystal system, shape	Ref.
Euclea natalensis roots	Zirconyl chloride octahydrate	50 g L⁻¹, 0.03 mol L⁻¹, 1:1	–, 3 h	105 °C for 24 h, 550 °C for 3 h	5.25–41.71 nm, –	Monoclinic and tetragonal, spherical	57
Acalypha indica leaves	Zirconyl chloride octahydrate	100 g L⁻¹, 0.1 mol L⁻¹, 1:5	80 °C, 2 h	200 °C for 2 h, –	58–72 nm, –	Monoclinic, –	60
Azadirachta indica leaves	Zirconyl chloride octahydrate	100 g L⁻¹, 50 mol L⁻¹, –	50–60 °C, –	120 °C, 600 °C for 5–6 h	–, –	–, –	61
Aloe vera leaves	Zirconium oxychloride octahydrate	500 g L⁻¹, 0.4 mol L⁻¹, –	Room temperature, 4 h	–, 500 °C	27.4 nm, 50 nm	Tetragonal, spherical	67
Eucalyptus globulus leaves	Zirconium oxychloride	100 g L⁻¹, 0.0098 mol L⁻¹, 1:1	–, 2–3 h	80 °C, 600 °C for 3 h	9–11 nm, –	Monoclinic and cubic, spherical	68
Lagerstroemia speciosa leaves	Zirconium nitrate	150 g L⁻¹, 0.2 N, 1:1	90 °C, 3 h	–, –	–, 56.8 nm	Tetragonal, –	65
Curcuma longa tuber	Potassium hexafluoro zirconate	25 g L⁻¹, 0.00098 mol L⁻¹, –	25 °C, 72 h	–, –	–, 41–45 nm	Monoclinic, –	62
Citrus aurantiifolia fruit	Zirconium(iv) acetate	10–30 mL, 0.038 mol L⁻¹, –	90 °C, 3 h	–, 750 °C for 2 h	21 nm, 20 nm	Cubic, –	69
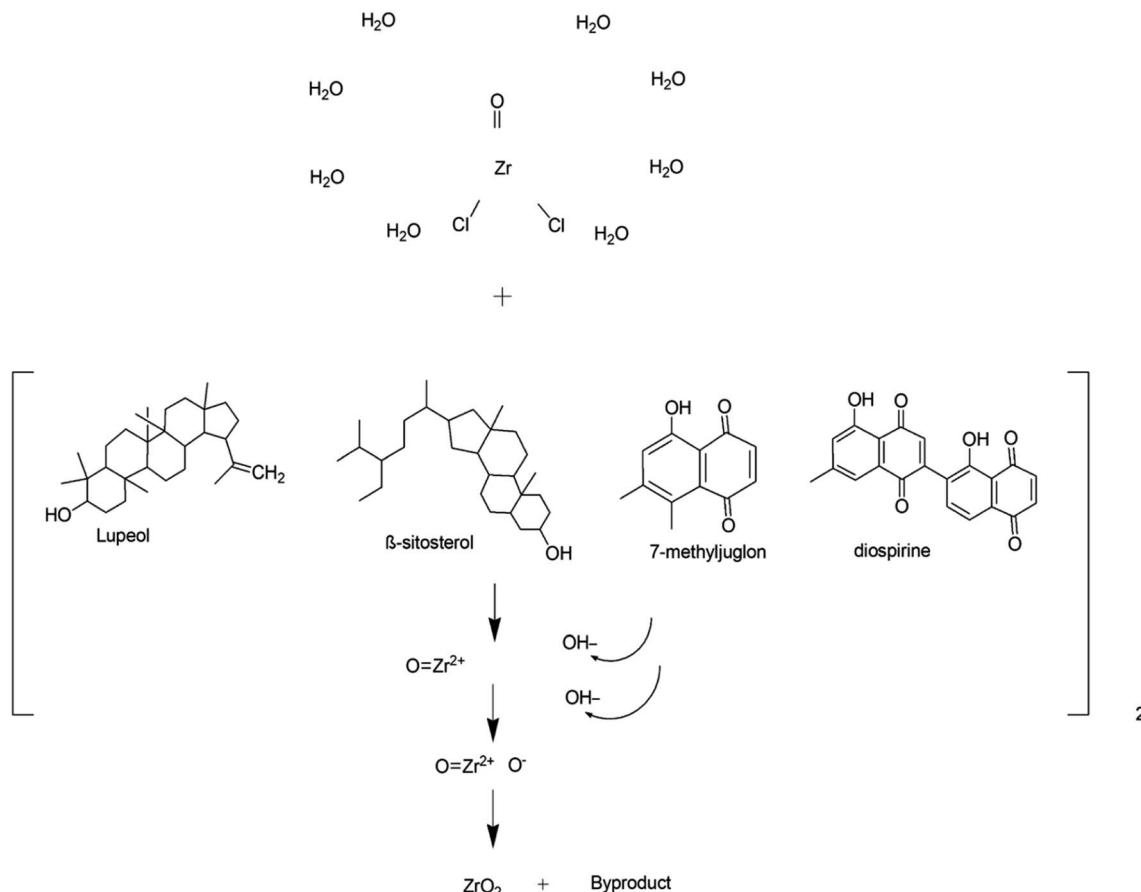
Fig. 5 Proposed reaction mechanism of synthesis of zirconia nanoparticles.[57]

monitoring the degradation of an azo dye using sunlight and reported excellent photocatalytic degradation of up to 94.58%.

It can be pointed out from the data listed in Tables 2 and 3 that zirconia nanomaterials prepared *via* greener routes (plant and microorganism-mediated methods) were found to have mainly pure phases either monoclinic or tetragonal. However, small particles having sizes in the range of 6–9 nm can be observed in all kinds of crystal systems known for zirconia. Interestingly, in almost all the instances of microorganism-mediated synthesis, heat treatment was not given which is surprising as merely the use of enzymes and proteins for the transformation of the zirconium precursor into zirconia could not yield fruitful results under *ex situ* conditions. However, in most of the plant-mediated synthesis, heat treatment in the temperature range of 60–120 °C of the reaction mixtures as well as in the range of 300–400 °C of the reaction product was given to obtain ZrO_2.

1.2 Applications of zirconia and its nanocomposites

New emerging and greener pathways for the preparation of metal-based nanomaterials have also unwrapped the significant applications of nanoscale zirconia in catalysis, adsorption, sensing, and dentistry. These applications have been discussed below.

1.2.1 Catalysis. Nanocatalysis involves nanomaterials as either a homogeneous or a heterogeneous catalyst for the reactions, and has shown exceptional growth during the past decade owing to the high surface-to-volume ratio and larger number of catalytic sites as compared to bulk materials.[146] Zirconia-based nanomaterials have been used as catalysts for transesterification and esterification (Table 4). In the light of zirconia nanoparticles as catalysts, Nor *et al.*[70] prepared a zirconia-based heterogeneous catalyst and employed it for the transesterification of waste cooking oil. In this study, the zirconia was modified with different salts (nitrates of Mg, Ca, Sr, Ba) using the wet-impregnation method. The Sr/ZrO_2 (2.7 wt% of Sr loading to ZrO) catalyst exhibited an appropriate concentration of basic as well as acidic site concentrations along with high pore volume, surface area as well as pore diameters. This catalyst produces biodiesel with a yield of 79.7%. Similarly, Qiu *et al.*[71] prepared a zirconia-based solid nanocatalyst having size in the range of 10–40 nm and potassium bitartrate as active sites for transesterification of soybean oil. In the follow-up study by Das *et al.*,[72] a monodisperse sulfated zirconia-based nanocatalyst (7.0–9.0 nm) was synthesized and employed for biodiesel production. In this study, biodiesel with 100% yield was obtained with a slight loss of catalytic activity. A similar kind of strategy was also followed in a report by Zhang *et al.*[73] where chlorosulfonic acid-modified zirconia was used as an efficient

Table 4 Zirconia-based heterogeneous catalysts for transesterification and esterification

Reactants	Catalyst	Methanol to oil molar ratio	Reaction temperature (°C) and time	Catalyst loading	Type of reaction	Conversion/yield	Ref.
Waste cooking oil and methanol	Sr/ZrO$_2$	29 : 1	115.5 °C, 169 min	2.7%	Transesterification, esterification	79.7%	70
Soybean oil and methanol	C$_4$H$_4$O$_6$HK/ZrO$_2$	16 : 1	60 °C, 2.0 h	6%	Transesterification	98.03%	71
Oleic acid and methanol	Chlorosulfonic acid modified zirconia	8 : 1	100 °C, 12 h	3%	Esterification	~100%	73
Refined soybean oil and methanol	CdO/ZrO$_2$	40 : 1	135 °C, 3 h	7%	Transesterification	97%	75
Silybum marianum oil and methanol	KOH/ZrO$_2$	15 : 1	60 °C, 2 h	6%	Transesterification	90.8%	74
Tannery waste sheep fat and methanol	Ferric-manganese-doped sulfated zirconia	15 : 1	65 °C, 300 min	8%	Transesterification	98.7%	76
Oleic acid and jatropha oil	SO$_4$$^{2-}$/Zr-KIT-6	20 : 1	120 °C, 6 h	4%	Esterification, transesterification	95%, 85%	78
Soybean oil and methanol	Mesoporous sulfated zirconia	12 : 1	120 °C, 4 h	4%	Transesterification	94.9%	79
Soybean oil and methanol	Sulfated zirconia	20 : 1	150 °C, 6 h	3%	Transesterification	84.6%	80
Sunflower oil	Sulphated ZrO$_2$-MCM-41	9 : 1	60 °C, 30 min	5%	Esterification	96.9%	81
Soybean oil and methanol	ZrO$_2$-supported bamboo leaf ash (ZrO$_2$/BLA)	15 : 1	–, 30 min	12%	Transesterification	92.75%	82
Oleic acid and methanol	SO$_3$H@ZrP	9 : 1	65 °C, –	5.0%	Esterification	89%	95
Nannochloropsis sp. (lipid) and methanol	Bi$_2$O$_3$/ZrO$_2$(CTAB)	90 : 1	80 °C, 6 h	20%	Transesterification, esterification	73.21%	83
Soybean oil/tributyrin, and methanol	UiO-66	44 : 1.1/52 : 1.3 respectively	140 °C, 5 h/120 °C, 5 h respectively	0.1 g	Transesterification	98.5%, 99.3%	90
Oleic acid and methanol	UiO-66(Zr)-green, UiO-66(Zr)-NO$_2$-green, and UiO-66(Zr)-NH$_2$	39 : 1	60 °C, 4 h	6%	Esterification	86%, 90%, 97% respectively	91
Soybean oil and methanol	AILs/POM/UiO-66-2COOH	35 : 1	110 °C, 6 h	10%	Esterification, transesterification	95.8%	92
Tributyrin and methanol	Zr-MOFs-S	52 : 1.3	140 °C, 6 h	0.1 g	Transesterification	—	93
Oleic acid with methanol	ZrSiW/UiO-66	20 : 1	150 °C, 4 h	0.24 g	Esterification	98.0%	94

heterogeneous catalyst in contrast to sulfated zirconia and it could also be employed for a pre-treatment step of esterification of oleic acid; consequently, saponification and catalyst inactivation were avoided. Similarly, Takase et al.[74] investigated the transesterification of a non-edible oil (Silybum marianum) using KOH-impregnated zirconia NPs as a catalyst. Patil et al.[75] prepared zirconia-supported cadmium oxide via a co-precipitation approach and used it for the transesterification of soybean oil with methanol. The activation energy and yield of the reaction were found to be 41.18 kJ mol^{-1} and 97% respectively under optimum conditions. Booramurthy et al.[76] investigated a sulfated zirconia nanocatalyst for transesterification using tannery waste sheep fat. Lin et al.[77] demonstrated the aqueous phase synthesis of ZrO_2 nanoparticles (5–10 nm) having Lewis acidic sites and employed it for the preparation of biofuel from jatropha oil. In this study, it was demonstrated that ZrO_2 nanoparticles have a higher capacity for phospholipid adsorption in contrast to commercial ZrO_2 powder owing to their higher surface area. Gopinath et al.[78] demonstrated the preparation of mesoporous sulfated Zr-KIT-6 via a hydrothermal route and employed it as a catalyst for the production of biodiesel. In this study, biodiesel was prepared by the esterification of oleic acid oil and transesterification of jatropha oil. This catalyst was significantly acidic due to the presence of Zr and sulphation, which resulted in an increase in activity for both transesterification as well as esterification. The prepared catalyst showed good stability and reusability and could be recycled up to three times. Similarly, Luo et al.[79] investigated the suitability of mesoporous sulphated zirconia NPs as an acidic catalyst to prepare biodiesel. In this study, the sulfated zirconia nanomaterial was prepared by a one-step liquid-crystal template method, where sodium dodecyl sulfate acted as a template and

sulfonating agent which improved the catalytic performance for transesterification. It was observed that higher calcination temperature resulted in the loss of catalytic activity such as loss of sulphate species, significant loss of acid sites, and the increased transformation of tetragonal zirconia into monoclinic zirconia, and reduced the surface area. Shi et al.[80] prepared the sulfated t-zirconia catalyst having super acidic sites by directly impregnating ammonium persulphate followed by calcination at 500 °C. It was employed as a catalyst for the preparation of biodiesel and demonstrated excellent yield (84.6%). Dehghani et al.[81] prepared a nanocatalyst using nano-sulfated zirconia supported over MCM-41 via an ultrasound-assisted impregnation/hydrothermal hybrid approach. The prepared catalyst showcased excellent activity to produce biodiesel (96.9%). Fatimah et al.[82] reported a heterogeneous ZrO_2 catalyst using bamboo leaf ash as a support for transesterification. Rahman et al.[83] investigated the zirconia based bifunctional heterogeneous nano catalysts $ZrO_{2(P123)}$ and $ZrO_{2(CTAB)}$ for the conversion of microalgae to biodiesel. Surfactant-assisted sol–gel method was followed to obtain high surface area catalyst. The introduction of Bi_2O_3 on zirconia enhanced the density of total acidic and basic sites of the catalyst. A possible mechanism for the simultaneous reactions using the bifunctional acid–base zirconia catalyst for biodiesel production is depicted in Fig. 6.

Metal organic frameworks (MOFs) constitute a new emerging class of porous materials. However, these materials are still in early stages of development and gradually progressing towards diverse applications such as catalysis, drug delivery, fluorescence sensing, etc. Zr based metal organic frameworks (Zr-MOFs) are most likely considered as encouraging MOF materials owing to their excellent physico-chemical properties and outstanding chemical stability. In 2008, an extraordinary
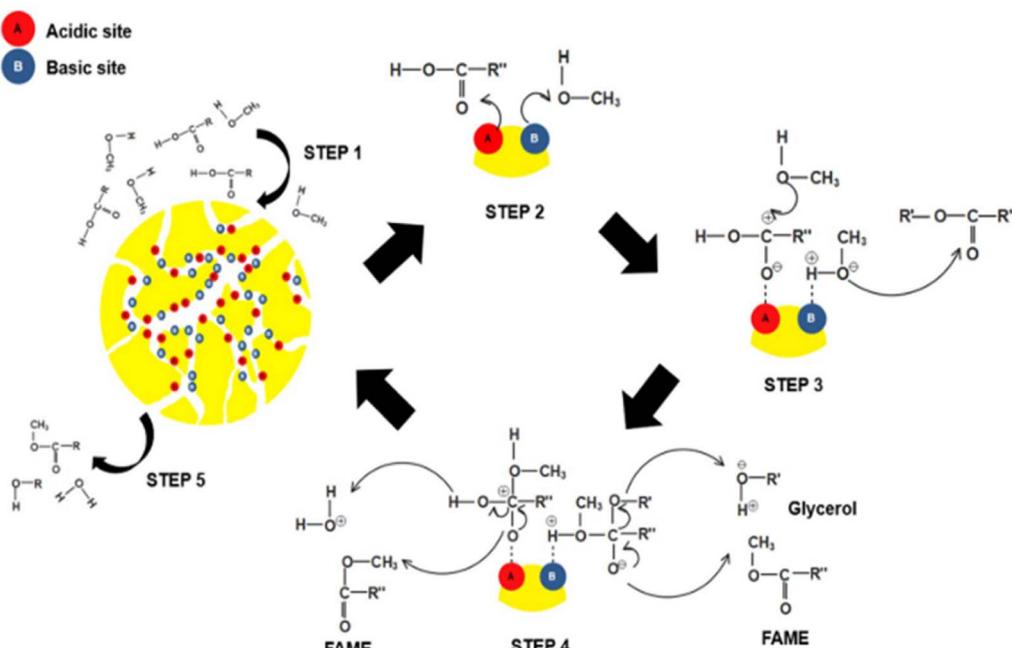
Fig. 6 The reaction mechanism of biodiesel production using a bifunctional acid–base catalyst.[83]

© 2022 The Author(s). Published by the Royal Society of Chemistry

discovery was made by Cavka et al.,[84] wherein 12-coordinated $Zr_6(\mu_3\text{-}O)_4(\mu_3\text{-}OH)_4(CO_2)_{12}$ clusters were synthesized, commonly referred to as UiO-66. It was found that the chemical and hydrothermal stability of UiO-66 was much higher than that of the other reported MOFs.[85–88] Since then, extensive efforts have been dedicated for the synthesis of Zr based MOFs, and the investigation of their properties, structures, functions and applications has been carried out intensively.

Schaate et al.[89] described the very first example of employing a modulated fabrication approach to prepare Zr based MOFs and studied the effects of different modulators such as acetic acid, water and benzoic acid on the formation of Zr-MOFs. Interestingly, it was found out that among all modulators, only benzoic acid affected the synthesis process; as its concentration was increased, bigger and quite distinct crystals were expected to form from the intermediates of UiO-66. Hence, the first large single crystals of Zr-MOF were obtained by this strategy, as confirmed by the single-crystal XRD technique. An interesting study by Zhou et al.[90] revealed the catalytic activity of UiO-66 prepared by using terephthalic acid and $ZrCl_4$. The catalyst demonstrated excellent recyclability for the preparation of bio-diesel using tributyrin and soybean oil with methanol. The performance of the catalyst was significantly dependent upon linker defects under different reaction parameters. Similarly, Abou-Elyazed et al.[91] reported the use of UiO-66(Zr)-green, UiO-66(Zr)-NO$_2$-green, and UiO-66(Zr)-NH$_2$ green for the preparation of biodiesel. Among all these MOFs, UiO-66(Zr)-NH$_2$ is found to be an efficient catalyst with an activation energy of 15.13 kJ mol^{-1}. Xie et al.[92] demonstrated a one-pot preparation of bio-diesel from low-cost acidic vegetable oils by using the AILs/POM/UiO-66-2COOH catalyst with 95.8% conversion of oil under optimized conditions. The obtained catalyst exhibited various merits such as good activity, higher surface area, reus-ability up to 5 cycles, and tolerance to high amounts of free fatty

acid (9 wt%) and water (3 wt%) in the feedstock. Lu et al.[93] synthesized sulphated Zr-based MOFs which had flower-like mesoporous nanosheets of zirconium and sulphate. In this study, the catalyst exhibited excellent activity, larger surface area (186.1 m^2 g^{-1}), and recyclability for the transesterification reaction. Recently Zhang et al.[94] prepared a ZrSiW/UiO-66 metal–organic framework by a hydrothermal method and used it for the biodiesel production. The prepared catalyst exhibited good activity, high surface area, and showcased heterogeneous nature as per the mechanism depicted in Fig. 7.

It is manifested from the literature cited in Table 4 that zirconia-based nanomaterials with enhanced acidity (sulphated zirconia) have been investigated extensively as a catalyst for simultaneous transesterification and esterification. However, a comparatively higher temperature and molar ratio of meth-anol to oil is required for the high yield of the reaction in contrast to the catalyst with enhanced basic sites (zirconia modified with KOH). Therefore, exploring Zr-based MOF and composites with basic sites could result in an efficient catalyst for transesterification.

1.2.1.1 Photocatalysis. ZrO_2, which is a semiconductor having a broad direct bandgap and high negative value of the conduction band, has also been used as a photocatalyst due to its suitable thermal stability, and optical and electrical proper-ties. It has been used as a photocatalyst for the degradation of organic water pollutants such as antibiotics and dyes. In Table 5, key parameters for the photocatalytic reactions using ZrO_2-based photocatalysts have been summarized. As can be seen in Table 5, there is variation in the photocatalytic activity of zirconia even for the same dye owing to different particle sizes and consequent different band gaps. Therefore, lights from both UV and visible region have been employed with ZrO_2 for the photocatalytic reactions. For instance, Ajabshir et al.[96] demonstrated the photocatalytic oxidation of the Eriochrome
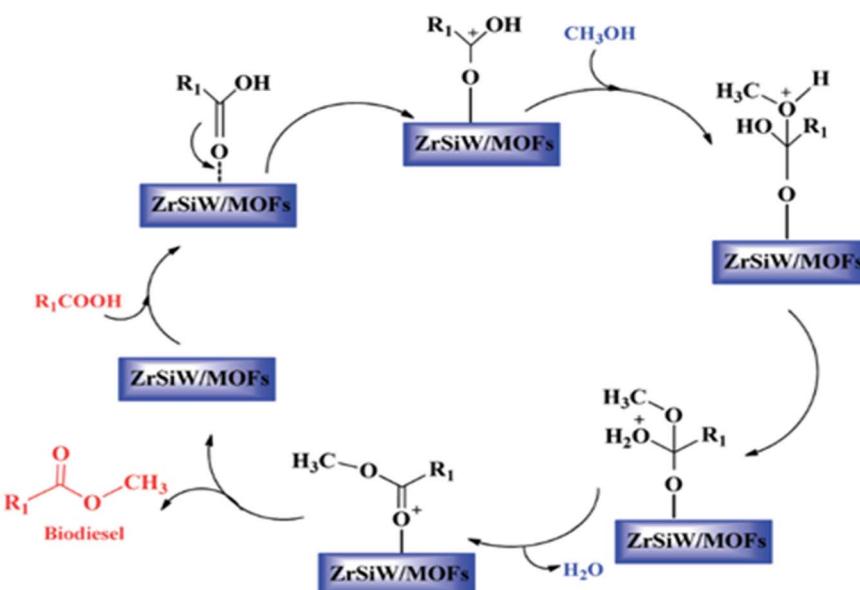
Fig. 7 Possible mechanism of esterification.[94]

Black T dye using sphere-like ZrO_2 NPs under UV light. On the other hand, star-like ZrO_2 NPs exhibited selective photocatalytic activity for the degradation of rhodamine B, methyl orange, and Congo red under visible light.[30] The mesoporous form of zirconia also demonstrated photocatalytic activity under the illumination of visible light for the degradation of tetracycline.[97] The $^•O_2^-$ and h^+ radicals were found to be accountable for the degradation of tetracycline. In another interesting report, Basahel et al.[98] proposed a mechanism (Fig. 8) for the degradation of methyl orange using zirconia nanostructures in varied crystalline forms, viz., monoclinic, tetragonal, and cubic. The monoclinic zirconia showed relatively higher photocatalytic activity than the other phases (tetragonal and cubic) due to the high crystallinity, large pore size distribution, oxygen-deficient zirconium oxide phase, and high density of surface hydroxyl groups. It involved the adsorption of methyl orange onto the surface of the nanoparticles. The exposure to UV light resulted in the formation of electron–hole pairs which react with the dissolved oxygen molecules and surface hydroxyl groups to form superoxide anion radicals and reactive hydroxyl radicals respectively.

As can be seen in Table 5, different sizes of ZrO_2 NPs and their nanocomposites have been used for the degradation of different dyes. Therefore, a clear conclusion about their photocatalytic activity can't be drawn directly. However, a generalization on the band-gap which is responsible for photocatalysis can be made. The lowest band gap of ZrO_2 was observed in its composites with reduced graphene oxide followed by that for the pure ZrO_2 NPs having a spherical shape and an average size of 17 nm. Thus, composites of small size ZrO_2 could further result in promising photocatalytic activities.

1.2.2 Anti-bacterial and anti-cancer activity. The use of ZrO_2-based nanomaterials in some biomedical solutions such as dentistry and drug delivery has been identified as an innovative approach owing to their low cost and less toxic nature. Therefore various biological properties, viz. antibacterial, antifungal, anticancer, and antioxidant, of zirconia-based structures have been investigated.[47,65,67,68] The important properties and key advancements are summarized below.

Gowri et al.[67] synthesized zirconia nanoparticles of 50–100 nm using leaves of aloe vera and investigated their antimicrobial and antifungal properties. Abdul et al.[59] demonstrated excellent antifungal and antibacterial properties of ZrO_2 NPs against F. moniliforme, F. graminearum, E. coli, and S. aureus. Similarly, Imran et al.[104] prepared Fe_3O_4-doped ZrO_2 nanoparticles of average size ~23 nm by the microwave method and investigated their antimicrobial activity. These nanoparticles (NPs) were used as dental fillers. Kumaresan et al.[105] demonstrated the antibacterial activity of zirconia NPs against Bacillus subtilis, Escherichia coli, and Salmonella typhi. The authors used marine brown alga, Sargassum wightii for the synthesis of zirconia nanoparticles having the size of ~4.8 nm. Masim et al.[106] prepared a polyaniline zirconia (PANI-ZrO_2) composite and employed it for the treatment of wastewater. The obtained composite showed antibacterial and anti-corrosion activity and acted as a phosphate adsorbent material.

Table 5 Photocatalytic activities of greener ZrO_2-based nanomaterials

Nanomaterial	Band gap (eV)	Average size (nm), shape, size range (nm)	Light source	Dye	Time of irradiation (min)	Degradation (%)	Ref.
ZrO_2	3.78	17, spherical, –	Sunlight	RY 160	120	94	99
ZrO_2	4.9	15, spherical, 10–18	UV light	Methylene blue and methyl orange	240	91, 69	100
ZrO_2	—	56.8, oval, –	Sunlight	Methyl orange	290	94.58	65
$ZnO–ZrO_2$	3.96, 3.99, 3.97, and 4.01	79.56, 98.78, 54.86, and 67.43, –, –	Solar light	Rhodamine 6G	330	98.94	101
Mg-doped ZrO_2	Varied	–, aggregated spherical, tetragonal and hexagonal, –	UV light	Rhodamine B	60	93	8
Reduced graphene oxide–ZrO_2	3.25	–, –, –	Sunlight	Reactive Blue 4	120	93	102
V_2O_5/ZrO_2	3.93	34–50	Solar light	Methyl orange and picloram	75	76.94% and 86%	103
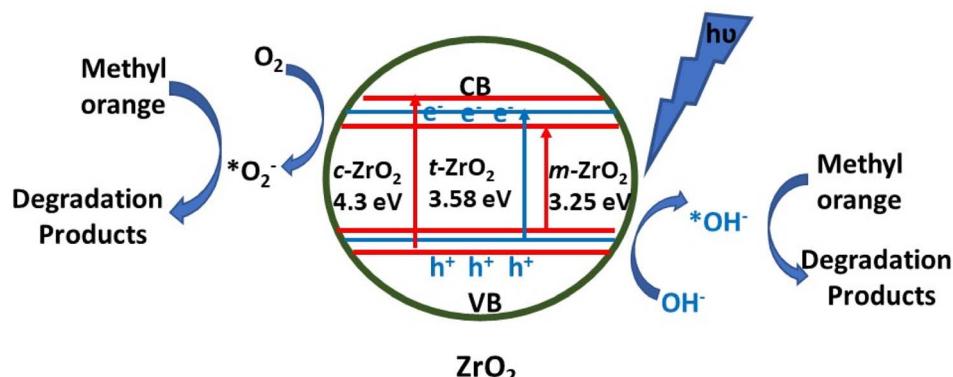
Fig. 8 Schematic representation of the processes leading to photocatalytic degradation.[98]

Fathima *et al.*[107] reported the fabrication of zirconia nano-particles having sizes in the range of 15–21 nm and investigated their antimicrobial activity. In this study, they identified antimicrobial activity against Gram-positive (*Bacillus subtilis* and *Staphylococcus aureus*) and Gram-negative bacteria (*Escherichia coli* and *Pseudomonas aeruginosa*), and found superior inhibitory activity against *Pseudomonas aeruginosa* at the concentration of 100 μg mL^{-1}. The antimicrobial activity of ZrO$_2$ NPs for different bacterial species is listed in Table 6. In another study, ZrO$_2$–ZnO nanoparticles were prepared by the sol–gel method and further evaluated for their antibacterial activity.[108] The mechanism of antibacterial activity by ZrO$_2$ NPs was proposed by Asha *et al.*[43] against *Pseudomonas aeruginosa* due to the rapid attraction between the negatively charged cell walls of *Pseudomonas aeruginosa* and positively charged zirconia NPs. Khan *et al.*[109] prepared glutamic acid-functionalized ZrO$_2$ NPs by using a solvothermal method and studied their antimicrobial activity against four strains of oral bacteria, *viz.*, *Streptococcus mutans*, *Rothia dentocariosa*, *Streptococcus mitis*, and *Rothia mucilaginosa*. The alteration of the surface of ZO$_2$ with glutamic acid increases the dispersion characteristics of nanoparticles in an aqueous medium which in turn possibly increases interactions between bacteria and nanoparticles.

Derbalah *et al.*[110] reported antifungal activity against *Rhizoctonia solani* which is known to be responsible for root rot in cucumber. The induction of resistance was examined using a real-time polymerase chain reaction. A concentration of 100 μg L^{-1} of zirconia nanoparticles showed better inhibition to improve the growth of the cucumber plant than the untreated cucumber plant. Ahmed *et al.*[53] reported the synthesis of biogenic ZrO$_2$ NPs by using *Enterobacter* sp. and studied their antifungal activity against *P. versicolor* (Fig. 9). In this study, nanoparticles ruptured the cells of pathogens by getting absorbed on the cell membrane and demonstrated a significant inhibition zone at the concentration level of 20 μg mL^{-1}. Similarly, Balaji *et al.*[68] demonstrated the synthesis of spherical zirconia nanoparticles (~9 to 11 nm) by using the leaf extract of *Eucalyptus globulus*. In this study, the antioxidant activity of the prepared material was also investigated using human colon carcinoma (HCT-116) and human lung carcinoma (A-549) cell lines by DPPH assay. The antioxidant studies of the prepared

zirconia NPs displayed significant inhibition (85.6%) at the concentration level of 158.15 μg mL^{-1}. The cytotoxicity of the prepared ZrO$_2$ was also investigated against HCT-116 colon cancer and A-549 lung cancer cell lines. A mechanism for the action of ZrO$_2$ towards cytotoxicity is also given in this report where ROS have been identified in key roles (Fig. 10). Furthermore, the anticancer activity of zirconia-based nanomaterials against various cell lines, and their % reduction in cell viability are summarized in Table 7.

Based upon data listed in Tables 3 and 5, it can't be concretely concluded that a particular phase of zirconia would be highly efficient for antibacterial and anticancer activity as most of the studies have been carried out on different microorganisms and cell lines by different methods. However, *prima facie*, the tetragonal phase seems to be more efficient as it had shown antibacterial activity on a range of microorganisms and significant anticancer activity on a range of cell lines. But, composites of zirconia with silver or yttria or iron oxide have shown promising results for both antibacterial as well as anticancer activities. Probably, composites of the tetragonal phase of zirconia could show enhanced superior activities.

1.2.3 Adsorption. Zirconia-based nanomaterials offer a significant prospect for efficient adsorption of toxins (dyes/organic and inorganic pollutants) in wastewater treatment because they could be designed with high specific surface area, sorption active sites, small particle size, and porous structure as compared to their bulk counterparts. Such materials have been employed as adsorbents for the adsorption of various types of pollutants including dyes such as methylene blue *etc.*, heavy metal ions such as arsenic, phosphates, vanadium ions, and pharmaceutical intermediates and products from aqueous solutions. The key parameters and optimized reaction conditions from recent reports on zirconia-based adsorbents have been summarized in Table 8. Debnath *et al.*[66] demonstrated the removal of tetracycline from wastewater by using zirconia nanoparticles under an optimized pH of 6.0 and an equilibrium time of 15 min as per the scheme given in Fig. 11. In this study, the mechanism of adsorption involves strong electrostatic interaction between the protonated surface of ZrO$_2$ NPs and the zwitterion of tetracycline. The adsorption capacity of ZrO$_2$ NPs was found to be 526.32 mg g^{-1}. Ghosh *et al.*[115] synthesized

Table 6   Antimicrobial activity of zirconia-based nanomaterials

| Zirconia-based nanomaterial, phase, shape, average size (nm), size range (nm)	Method	Microorganism	% Activity	Inhibition zone	Applications	Ref.
ZrO$_2$, tetragonal, spherical, –, 50–100	Agar diffusion method	S. aureus, E. coli (bacteria) and C. albicans, A. niger (fungus)	—	23, 33, 22, 18 mm respectively	—	67
Fe$_3$O$_4$-doped ZrO$_2$, tetragonal, spherical, 30	Agar well diffusion method	Bacillus subtilis (bacteria)	—	32 mm	Dental fillers	104
ZrO$_2$, –, spherical, 5, –	Agar well diffusion method	Bacillus subtilis, E. coli, and Salmonella typhi (bacteria)	—	21, 19, 19 mm respectively	—	105
Polyaniline-ZrO$_2$, –, –, –, –	Agar diffusion method	E. coli and Staphylococcus aureus (bacteria)	—	14, 18 mm respectively	Used in the treatment of wastewater effluent and decontamination of rearing water	106
ZrO$_2$, monoclinic, spherical, 35, 32–38	Disc diffusion method	Pseudomonas aeruginosa, E. coli, Staphylococcus aureus, and Bacillus subtilis (bacteria)	—	10 mm in Pseudomonas aeruginosa	—	43
ZrO$_2$–ZnO, –, spherical, 26–34, –	Disc diffusion method	Bacillus subtilis, Streptococcus mutans, Staphylococcus aureus, E. coli, Pseudomonas aeruginosa, and Klebsiella oxytoca (bacteria)	—	—	—	108
Glutamic acid functionalized zirconia (GA-ZrO$_2$), cubic, spherical, 2.5, –	Autoclaved brain heart infusion broth (BHI) or agar	Rothia mucilaginosa, Rothia dentocariosa, Streptococcus mitis, and Streptococcus mutans (bacteria)	58% ± 4.9% (R. dentocariosa) 52% ± 2.9% (Streptococcus mutans)	—	—	109
ZrO$_2$, –, spherical, –, 15–21	Disc diffusion method	Bacillus subtilis, Staphylococcus aureus, E. coli and Pseudomonas aeruginosa (bacteria)	—	20 mm in Pseudomonas aeruginosa	Anti-tooth decay applications	107
ZrO$_2$, tetragonal, –, 17, –	Agar dilution method	Rhizoctonia solani (fungus)	86.6%, 100 µg L^{-1}	—	Improved cucumber growth	110
ZrO$_2$, –, spherical, –, 33–75	Agar well diffusion	Pestalotiopsis versicolor (fungus)	—	25.18 ± 1.52 mm	Protects bayberry (twig blight disease pathogen) plants against antifungal agents	53
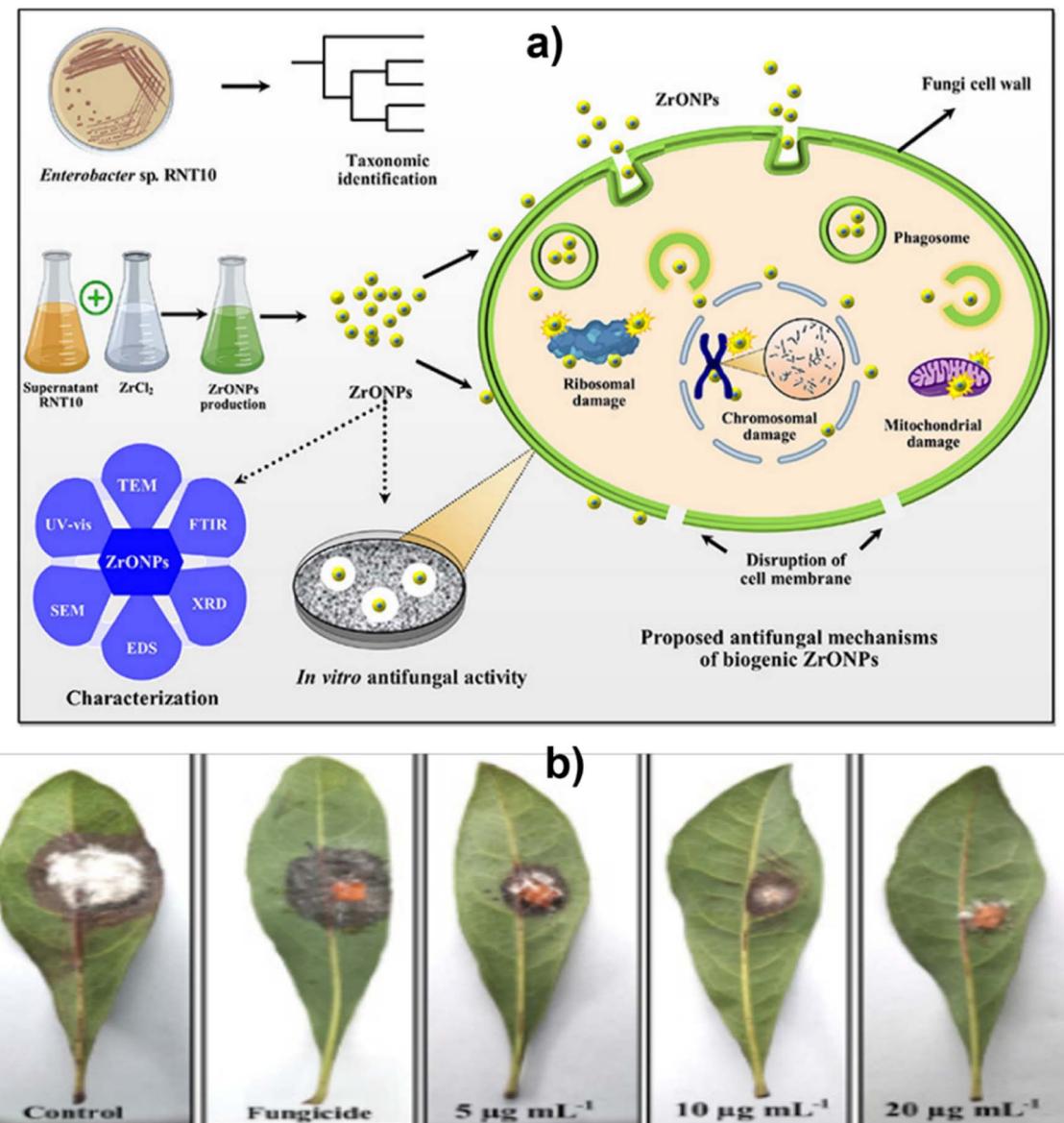
Fig. 9 (a) Green synthesis and characterization of zirconium oxide nanoparticles by using a native *Enterobacter* sp. and its antifungal activity against bayberry twig blight disease pathogen *Pestalotiopsis versicolor* and (b) effect of various concentrations of ZrO NPs on bayberry leaves infected with *P. versicolor* strain XJ27. Adapted from ref. 53 with permission from Elsevier, copyright 2020.

a ceria-incorporated ZrO_2 nanocomposite having a particle size of ∼50 nm and employed it for the removal of arsenic(III) from the aqueous phase. The prepared material offers its surface for the oxidation of arsenic(III) to arsenic(V). It showed a kinetically pseudo-second-order reaction and the obtained Langmuir isotherm indicated a monolayer adsorption capacity of 17.07 mg g^{-1}.

It can be suggested from the literature summarized in Table 8 that both bare ZrO_2 and its composites could be employed for the adsorption of pollutants from effluents effectively. Specifically, designing composites of ZrO_2 NPs with graphene oxide could be a useful approach for fabricating economical and efficient adsorbents for a range of pollutants and industrial-by-products.

1.2.4 Dentistry. Nanoscale ZrO_2 has increasingly become one of the significant ceramic materials in the field of dentistry due to its outstanding properties such as natural color, stable chemical properties, good corrosion resistance, high toughness, mechanical strength and, most importantly, its superior biocompatibility. It is being used as a dental implant biomaterial and dental crown. Zirconia-based ceramics are found to be chemically inert materials, therefore, considered preferable candidates for superb cell adhesion, and no unfavourable systemic reactions have been observed. Modification of the implant surface is highly necessary to increase its strength and prevent its failure caused due to insufficient bone formation and apposition. Methods such as sandblasting, acid etching, and laser etching have been performed for this purpose.[122]
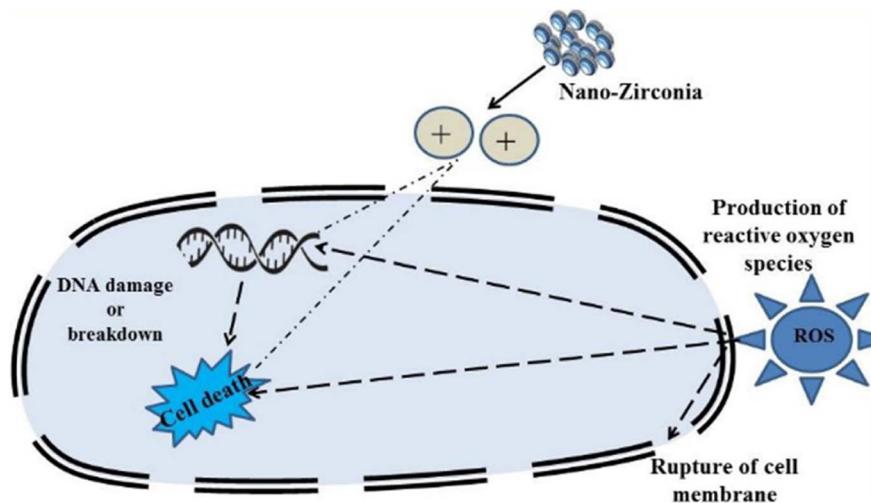
Fig. 10 Plausible mechanism of action by ZrO$_2$ NPs towards cytotoxicity. Adapted from ref. 68 with permission from Elsevier, copyright 2017.

Table 7 Anticancer activity of zirconia-based nanomaterials

Zirconia-based nanomaterial, phase, shape, average size (nm), size range (nm)	Method	Cell line	% Reduction in cell viability	Ref.
ZrO$_2$, tetragonal, spherical, –, 9–11	MTT	Human colon carcinoma (HCT-116) and human lung carcinoma (A-549) cell lines	50%	68
ZrO$_2$, tetragonal, tetragonal, 56.8, –	MTT	MCF-7 cell lines	18%	65
Fe$_3$O$_4$@ZrO$_2$, –, spherical, 155.23 ± 7.1, –	CCK-8 method	HepG2 cell line	54.76% ± 5.88% to 17.72% ± 3.66%	111
AgNPs@UiO-66(DMF), –, cubical, 140, –	MTT	SMMC-7721 and HeLa cells	92 and 89% respectively	112
Y$_2$O$_3$/ZrO$_2$, –, –, 33.9 ± 2.1, –	MTS and NRU	Human skin keratinocyte (HaCaT) cells	94%, 90%, 78% and 65% (in 24 h)	113
Sulphated zirconia, –, tetragonal, 43, 37–54	MTT	HT29, human breast cancer MCF-7, and human liver cancer HepG2	50%	114

Aivazi et al.[123] reported the laser method for the modification of the surface to support osseointegration. In this study, surface modification caused a positive impact on the viability of fibroblast L929 cells. Tahsili et al.[124] prepared meso-/micro-/nanoscale rough zirconia by solid-state laser sculpting for improving the performance of zirconia implants. The prepared zirconia shows a significant increase in osseointegration. Yu et al.[125] studied the effect of surface properties of nano-scale zirconia on the adhesion and biofilm development of Streptococcus mutans. In this study, it was observed that the surface roughness of the nanostructure can influence the adhesion force and early attachment (2 and 4 h) of Streptococcus mutans on the zirconia. Nevertheless, it did not affect the formation of biofilm in the later stages of 6, 8, 12, and 24 h.

Recently, an yttria-stabilized t-zirconia polycrystal material has been used for implants and dental applications due to its excellent mechanical properties.[7] Interestingly, zirconia-based nanomaterials can also be used to improve the physical and mechanical properties of polymethyl methacrylate (PMMA) which is a denture repair material. Gad et al.[126] also demonstrated that the tensile strength of PMMA could be increased

using zirconia nanoparticles and can be used as a denture base with reduced translucency. Lohbauer et al.[127] demonstrated the preparation of spherical ZrO$_2$ NPs in the range of 20–50 nm using laser vaporization. These nanomaterials were used as fillers in the dental adhesive.

Fathima et al.[107] synthesized zirconia nanoparticles and demonstrated their excellent antibacterial activity and anti-decay application on teeth. Bacteria may generate acids during their metabolic activities which result in the demineralization of teeth (Fig. 12). However, coating with zirconia NPs has shown resistance to acid attacks as well as remarkable activity against oral pathogens bearing negatively charged cell walls. The electrostatic interactions between positively charged nanoparticles and charged microorganisms inhibit the activities of microbes. Gad et al.[128] reported a novel method for denture stomatitis inhibition by using ZrO$_2$ nanoparticles owing to their antifungal activity. The authors investigated the inhibitory effect of ZrO$_2$ nanoparticles on Candida albicans adhesion to restore polymethyl methacrylate denture bases. Similarly, in another investigation by Oshima et al.,[129] a zirconia/alumina composite nanomaterial (Ce-TZP/Al$_2$O$_3$) was found to increase the

© 2022 The Author(s). Published by the Royal Society of Chemistry

Table 8   Zirconia-based nanomaterials as adsorbents

Adsorption activity	Zirconia nanomaterial type	Experimental conditions (temperature, pH, and equilibrium time)	Adsorption capacity	Isotherm	Ref.
Tetracycline from wastewater	ZrO_2	–, 6, 15 min	526.32 mg g^{-1}	Langmuir isotherm	66
Phosphate in treated wastewater	PANI-ZrO_2	–, 25 °C, 6.9, –	32.4 mg g^{-1}	Langmuir isotherm	106
Phospholipid adsorption from jatropha oil used for biofuel	ZrO_2	—	13.92 mg g^{-1}	Langmuir isotherm	77
Adsorption of methylene blue and tetracycline hydrochloride from water	UiO-66-$(OH)_2$/graphene oxide (GO)	298 K, 9, –	99.96% and 94.88%, respectively	Langmuir, Freundlich, Sips isotherm	116
Adsorption of arsenic(III) from the water	Ceria incorporated zirconia nanocomposites	303 K, 7.0, –	17.07 mg g^{-1}	Langmuir isotherm	115
Adsorption of chromium and dyes RB-21, RR-141, and Rh-6 G	Chitosan-zirconium phosphate nanostructures	303 K, –, –	311.53 mg g^{-1}, 457 mg g^{-1}, 435.1 mg g^{-1} and 438.596 mg g^{-1} respectively	Langmuir isotherm	117
Adsorption of vanadium ion	CNZ@NCT/Zr	298 K, <5, –	277.75 mg g^{-1}	Langmuir isotherm	118
Adsorption of phosphate from water	ZrO_2/Fe_3O_4	–, neutral, –	29.5 mg g^{-1}	Langmuir isotherm	119
Adsorption of norfloxacin in water	UiO-66-NH_2	298 K, 6–8.5, 6 h	222.5 mg g^{-1}	Langmuir isotherm	120
Adsorption of toxic arsenite (As(III)) and arsenate (As(v)) from aqueous solutions	Mesoporous zirconia nanostructure	–, neutral, –	105.03 and 110.29 mg g^{-1}, respectively	Langmuir isotherm	121
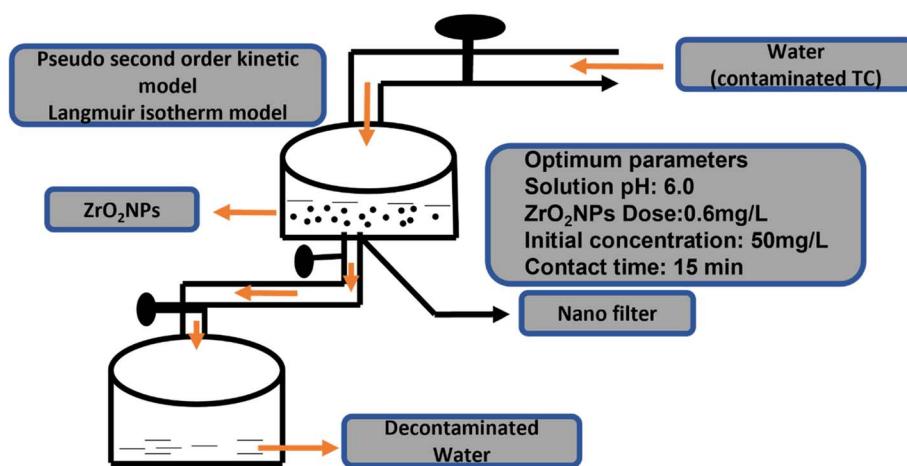
Fig. 11   Schematic diagram of batch adsorption of TC on the surface of biosynthesized ZrO_2 NPs.[66]

osseointegration capability and osteogenic response of implants, where the surface of the nanostructured Ce-TZP/Al_2O_3 was modified by HF treatment.

Yamada *et al.*[130] prepared silver NP-coated yttria-stabilized ZrO_2 and investigated its antibacterial activity against oral pathogens such as *Staphylococcus aureus*, *Streptococcus mutans*, *Escherichia coli*, and *Aggregatibacter actinomycetemcomitans* (Fig. 13). The composite shows antimicrobial activity, particularly against *Escherichia coli*. The efficacy of the prepared material was tested *via* an accelerated aging test. In this test, the
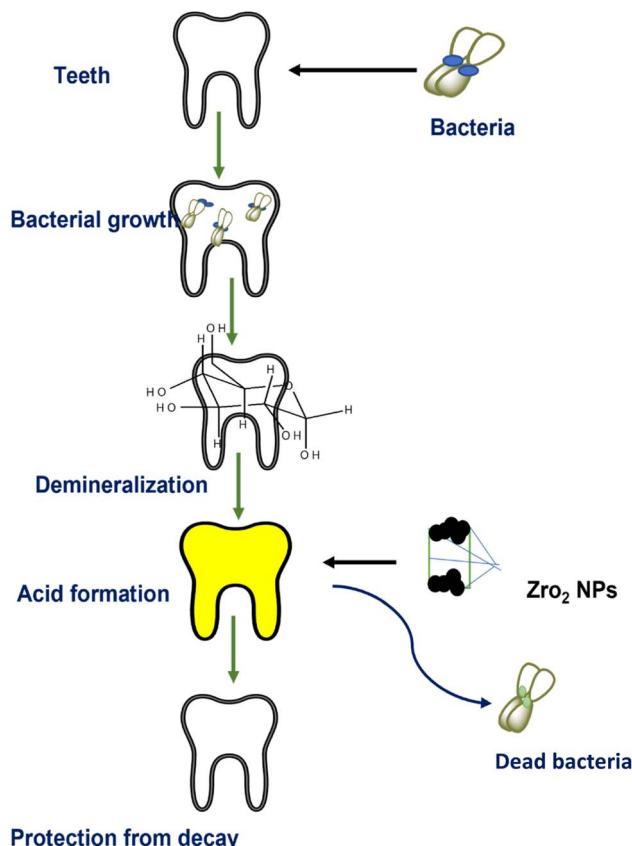
Fig. 12 Role of ZrO_2 NPs in dental care.[107]

release profile of silver NPs was investigated which was found to be less than 1 percent, hence the prepared material was found to be thermally stable. Therefore, it was suggested that the bactericidal action of the composite was due to its contact with the bacteria and not owing to the release of silver NPs. Thus, the prepared material could be further investigated for the treatment of dental caries and periodontal disease.

1.2.5 Sensing. Zirconia-based nanomaterials are also being explored for sensing applications due to their favorable electrochemical and physicochemical properties such as high surface area, chemical stability, and fluorescent nature. Various sensing parameters, modes of generating signals and

substances for which such materials have been employed have been summarized in Table 9. For instance, Zhang et al.[131] demonstrated the detection of trace amounts of ethanol using zirconia nanoparticles with high sensitivity. The developed sensor indicated a constant and stable response for 100 h via a chemiluminescence reaction and demonstrated remarkable durability. The formation of acetaldehyde as one of the possible luminescent intermediates was observed in the sensing process.

Garadkar et al.[132] fabricated thick film resistors using nanostructured ZrO_2 (25 nm) via the screen printing technique. The as-prepared resistor was used for the selective detection of H_2 gas and showed a significant signal at room temperature even in the presence of a smaller amount of H_2. It was reported that films exhibited a clear response to 50 ppm of H_2 in contrast to other gases at a higher amount of 1000 ppm. Chikere et al.[133] fabricated a zirconia nanoparticle modified carbon paste electrode and employed it for the electrochemical detection of gallic acid in a concentration range of 1×10^{-6} to 1×10^{-3} mol L^{-1}. The weak ionic interactions between the oxygen anions of zirconia nanoparticles (monoclinic) and positively charged graphite sheets, as depicted in Fig. 14, were found to stabilize the sensor. The designed sensor generated a signal via electrochemical oxidation of gallic acid and was employed for detection of the latter in red and white wine.

Wang et al.[134] prepared zirconia nanoparticles having an average size of 20 nm and employed them to make a thick film humidity sensor using a substrate. The prepared sensor showed a change in impedance from 10^6 to 10^2 Ω with an increase in relative humidity (RH) from 11 to 98%. In this report, the impact of temperature on the impedance of the sensor was evaluated and the conduction process of the sensor was explained using an equivalent circuit with resistors and capacitors. Gong et al.[135] fabricated a nanostructured composite of zirconia and graphene by solid-phase extraction. The prepared material afforded high recognition and enrichment for phosphoric moieties due to the NPs of ZrO_2, large surface area, and high conductivity owing to graphene nanosheets. The prepared material was successfully employed for the detection of methyl parathion via square-wave voltammetry.

Trinadh et al.[136] prepared an electrochemical sensor using graphene quantum dots (GQDs) and lanthanum doped zirconia
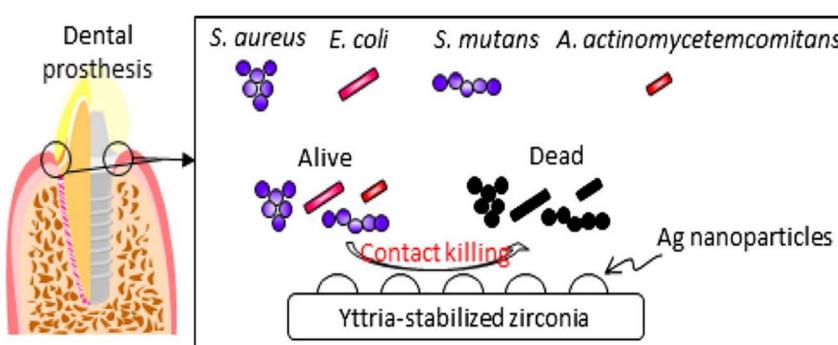
Fig. 13 Silver NP-coated zirconia for antibacterial prosthesis. Adapted from ref. 130 with permission from Elsevier, copyright 2017.

Table 9 Application of zirconia-based nanomaterials in sensing

Sensor	Synthesis method	Analyte	Working temperature	Recovery time, response time	Sensing technique	Limit of detection/linear response	Ref.
ZrO$_2$ on a silicon substrate	—	Humidity	10–30 °C	60 s, 130 s	Measurement of impedance	—	134
ZrO$_2$ NP decorated graphene nanosheets	Electrochemical approach	Methyl parathion	—	-, -	Square-wave voltammetry	0.6 ng mL^{-1}	135
Zirconia nanocubes	Hydrothermal method	Arsenic(III)	—	-, below 2 s	Cyclic voltammetry	5 ppb	29
Zirconia NPs	Precipitation method	Dimethyl amine	330 °C	-, less than 50 s	Cataluminescence	6.47 × 10^{-4} ng mL^{-1}	138
ZrO$_2$ 5%Y/ZrO$_2$ Ag-5% Y/ZrO$_2$	Hydrothermal method	CO$_2$	300–400 °C	22 s, –	Measurement of current	—	139
Polyaniline zirconia nanocomposite	Polymerization method	Esomeprazole	—	–, 9 s	Electrochemical impedance spectroscopy and cyclic voltammetry	97.21 ng mL^{-1}	140
Au-NPs/ZrO$_2$ nanofiber	Nonthermal spin-coated sol–gel method	Pesticide	—	–, –	Surface-enhanced Raman scattering	10^{-6} to 10^{-8} M	137
GQDs@La^{3+}@ZrO$_2$ nanoparticles	Bottom-up and sintering approach	Flutamide	Room temperature	—	Electrochemical signal	0.00082 μM	136
ZrO$_2$ NP modified carbon paste electrode	Hydrothermal method	Gallic acid	Room temperature	—	Differential pulse voltammetry (DPV)	1.24 × 10^{-7} mol L^{-1}	133
SiO$_2$ZrO$_2$ composite	Sol–gel method	NO$_2$	25 °C	Varied	Measurement of resistance	—	141

nanoparticles for the detection of flutamide in urine samples as per the scheme depicted in Fig. 15. For designing this sensor, La^{3+}@ZrO$_2$ was prepared by the coprecipitation method using a solution of zirconyl chloride and lanthanum nitrate as metal precursors and NH$_4$OH as the precipitating agent. The addition of NH$_4$OH decreases the pH of the solution which leads to the formation of precipitates. The obtained precipitates were washed with methanol and water, dried, and calcined at 600 °C. Finally, the glass carbon electrode-based sensor was fabricated by drop casting a suspension of 1.0 mg of GQDs and 1.0 mg of La^{3+}@ZrO$_2$ on a pre-treated GCE. In this study, the signal was generated due to the electrochemical reduction of flutamide (12 μM) in phosphate buffer solution (pH = 7).

Lee et al.[137] demonstrated the preparation of Au nanoparticle coated zirconia nanofibers and employed them as a surface-enhanced Raman scattering sensor for the detection of a variety of pesticide (carbaryl, phosmet, cypermethrin, and permethrin) residues in fruits or vegetables. In this study, nanofibers of zirconia were fabricated on a silicon wafer via the spin coating technique using a solution of ZrCl$_4$ in isopropanol. Afterward, gold NPs were deposited on ZrO$_2$ nanofibers via an electron beam evaporator. The prepared sensor shows excellent selectivity to organophosphates even in the presence of multiple pesticides. It was successfully employed for a practical application using diluted juice containing sliced pesticide-containing apple peels and could differentiate different pesticides.

The literature summarized in Table 9 revealed that ZrO$_2$ or its composites could be employed for designing a range of sensors based upon different techniques such as electrochemical, luminescence etc. However, significant LODs have been displayed by them via electrochemical signals. Specifically, a cyclic voltammetry-based signal from such sensors seems to be a more promising one owing to the electrical properties of ZrO$_2$.

2 Outlook and futuristic scope

Recently, there have been substantial efforts and significant developments in the field of synthesis of nanomaterials for better exploitation in numerous applications. With the aid of a modified outlook of nanomaterials and the comprehension of their potential in various industries, including, but not limited to, pharmaceuticals, textiles, paper, pulp, and drug delivery, the influx of zirconia nanoparticles has offered innumerable benefits and provided solutions for several continuing problems related to clinical diagnosis, catalysis, and dentistry, and can indefinitely offer long-term economic benefits. In the particular interest towards the synthesis of zirconia nanoparticles, several chemical and green methods have been developed and their plausible mechanisms have been studied in detail. Furthermore, efforts have also been made to achieve monodispersity, desired particle size, shape, and stability via tuning the reaction conditions and parameters. However, there are challenges associated with improving the efficiency of the synthesis and achieving the specific particle sizes and morphology, a desirable cubic phase, long-term stability, and reduced aggregation of particles. Moreover, expansion of the volume of particles with the cubic phase has also been observed
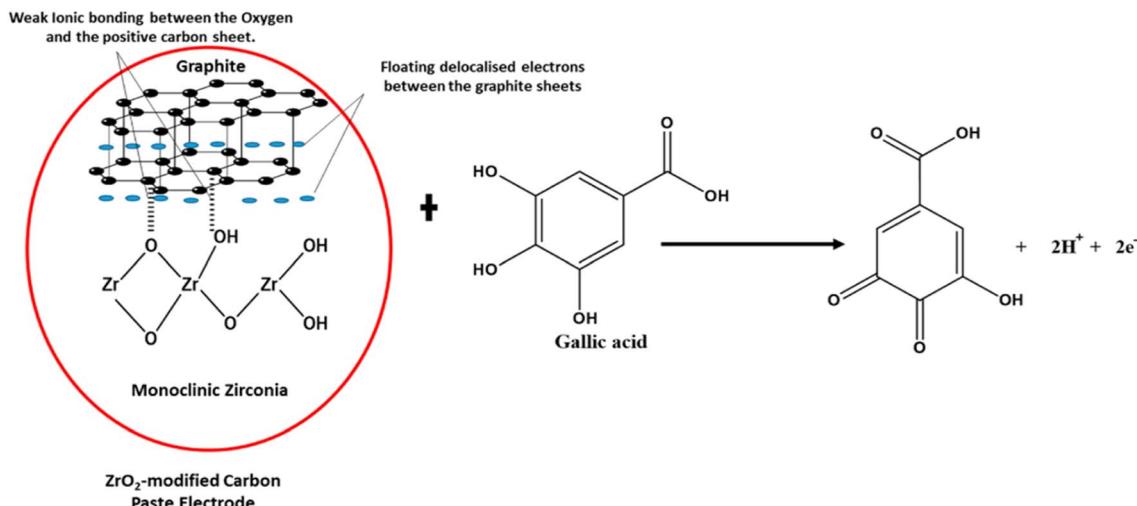
Fig. 14 Proposed interaction between ZrO$_2$ NPs and graphite, demonstrating a weak ionic bond between some of the oxygen and the positive graphite sheet in the electrochemical determination of gallic acid.[133]
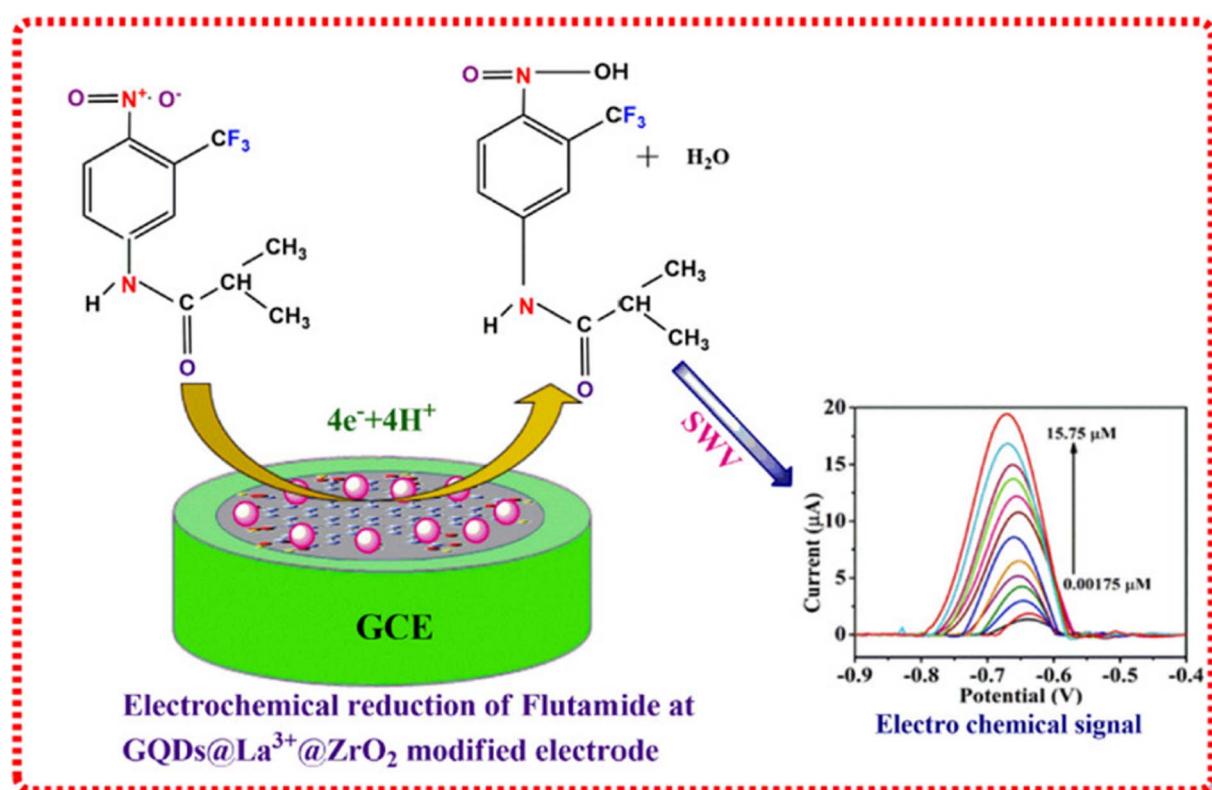
Fig. 15 Pictorial representation of the fabrication of GQDs@La^{3+}@ZrO$_2$@GCE. Adapted from ref. 136 with permission from Elsevier, copyright 2017.

when employed in high-temperature applications due to its transformation into the tetragonal phase and subsequently tetragonal to monoclinic phase which results in the generation of stress and cracks and makes the material unfit for applications. Therefore, a long journey is still pending in this direction to overcome the above-mentioned limitations. To gain an insight, a significant number of theoretical studies using density functional theory have been performed to understand

the structure, nature of surface sites, and stability of zirconia nanoparticles. Recently, Maleki *et al.*[142] performed DFT calculations to obtain the ^{17}O solid-state NMR chemical shifts for studying the nature of surface sites on zirconia. In an interesting study, Puigdollers *et al.*[143] showed that nanoparticles with partly truncated octahedral morphology display the highest stability. Moreover, nanoparticles with only stable facets {101} were found to be less stable due to the presence of reduced Zr,

thereby confirming that low-coordinated sites create defective states in the electronic structure and reduce the effective bandgap, which can result in enhanced interaction with deposited species and could modify the photocatalytic activity. In another report, the presence of acidic and basic sites on zirconia was investigated using DFT calculations for obtaining the IR and NMR spectra of adsorbed molecules (carbon monoxide and pyrrole). This study confirms the presence of acidic Zr sites and basic O^- sites in nanoparticles. However, further theoretical studies for obtaining stronger acidic and basic sites and achieving the stability of the cubic phase in zirconia nanoparticles could enhance the suitability of zirconia in various applications as discussed earlier. To ensure the commercial applicability of such materials in various technological applications, future perspectives should focus not only on an in-depth understanding of the surface structure and active sites but also on the design and development of well-defined chemical and green systems for the substantially controllable site environment and attractive characteristics.

Experimentally, two approaches have been employed to enhance the stability and applications of zirconia nanoparticles. The first one involves *in situ* modification with stabilizers and other metal oxides such as CaO, MgO, and Y_2O_3 during the preparation of the nanomaterials. Modification with another metal oxide could generate vacancies stimulating changes in the electronic and geometric environment that can further enhance the optical and electrical properties which is also supported by several theoretical studies.[143-145] The second strategy involves exploring greener methods with novel additives that could be employed. Although the synthesis of zirconia nanomaterials using plant extracts and microbes is considered to be clean, nontoxic, simple, and safe, there are only a few reports in this regard and sufficient efforts have not been made with diverse varieties of plants and microorganisms with different possible reaction pathways. Moreover, the combination of the sol–gel method and greener reactants is rarely reported. Specifically, the sol–gel method offers unique advantages such as good control over the structure and kinetics of the process. Moreover, fine control of the composition of a multicomponent nanomaterial could be achieved *via* this method as small quantities of dopants can be introduced in the sol and uniformly dispersed in the final product. Therefore, further improvising this method using greener ingredients by keeping in view the motive of increasing the strength and biocompatibility could result in the invention of new materials suitable for various applications such as dentistry, catalysis, sensors, *etc.*

Conflicts of interest

There are no conflicts to declare.

Acknowledgements

References

1 J. L. Gole, S. M. Prokes, J. D. Stout, O. J. Glembocki and R. Yang, *Adv. Mater.*, 2006, **18**, 664–667.

2 S. Zhuiykov and N. Miura, *Sens. Actuators, B*, 2007, **121**, 639–651.

3 G. D. Wilk and R. M. Wallace, *Appl. Phys. Lett.*, 2000, **76**, 112–114.

4 X. J. Jin, *Curr. Opin. Solid State Mater. Sci.*, 2005, **9**, 313–318.

5 S. Gupta, S. Noumbissi and M. F. Kunrath, *Med. Devices Sens.*, 2020, **3**, 1–8.

6 B. Tyagi, K. Sidhpuria, B. Shaik and R. V. Jasra, *Ind. Eng. Chem. Res.*, 2006, **45**, 8643–8650.

7 E. Camposilvan, F. G. Marro, A. Mestra and M. Anglada, *Acta Biomater.*, 2015, **17**, 36–46.

8 L. Renuka, K. S. Anantharaju, S. C. Sharma, H. P. Nagaswarupa, S. C. Prashantha, H. Nagabhushana and Y. S. Vidya, *J. Alloys Compd.*, 2016, **672**, 609–622.

9 E. Mustafa, M. Wilhelm and W. Wruss, *Ceram. Int.*, 2003, **29**, 189–194.

10 K. Anandan, K. Rajesh, K. Gayathri, S. Vinoth Sharma, S. G. Mohammed Hussain and V. Rajendran, *Phys. E*, 2020, **124**, 114342.

11 J. Liang, Z. Deng, X. Jiang, F. Li and Y. Li, *Inorg. Chem.*, 2002, **41**, 3602–3604.

12 A. Behbahani, S. Rowshanzamir and A. Esmaeilifar, *Procedia Eng.*, 2012, **42**, 908–917.

13 F. Heshmatpour and R. B. Aghakhanpour, *Powder Technol.*, 2011, **205**, 193–200.

14 E. Geuzens, G. Vanhoyland, J. D'Haen, M. K. Van Bael, H. Van Den Rul, J. Mullens and L. C. Van Poucke, *Key Eng. Mater.*, 2004, **264–268**, 343–346.

15 C. O. Kappe, *Angew. Chem., Int. Ed.*, 2004, **43**, 6250–6284.

16 A. K. Singh and U. T. Nakate, *Sci. World J.*, 2014, **2014**, 349457.

17 H. Yousaf, M. Azhar, M. Bashir, S. Riaz, Z. N. Kayani and S. Naseem, *Optik*, 2020, **222**, 165297.

18 B. S. Bukhari, M. Imran, M. Bashir, S. Riaz and S. Naseem, *J. Sol-Gel Sci. Technol.*, 2018, **87**, 554–567.

19 T. B. Riaz, K. B. Hadi and S. Naseem, *J. Mech. Behav. Biomed. Mater.*, 2020, **112**, 104012.

20 S. Mishra, A. K. Debnath, K. P. Muthe, N. Das and P. Parhi, *Colloids Surf., A*, 2021, **608**, 125551.

21 H. Zhou, S. Pu, J. Huo, W. Cao, B. Wang and J. Li, *Ceram. Int.*, 2016, **42**, 15005–15011.

22 S. Sagadevan, J. Podder and I. Das, *J. Mater. Sci.: Mater. Electron.*, 2016, **27**, 5622–5627.

23 T. Ahmad, *Mater. Sci. Eng. Int.*, 2017, **1**, 4–8.

24 S. D. Meetei and S. D. Singh, *J. Alloys Compd.*, 2014, **587**, 143–147.

25 H. J. Noh, D. S. Seo, H. Kim and J. K. Lee, *Mater. Lett.*, 2003, **57**, 2425–2431.

26 H. M. Abdelaal, *Mater. Lett.*, 2018, **212**, 218–220.

27 S. Nath, A. Biswas, P. P. Kour, L. S. Sarma, U. K. Sur and B. G. Ankamwar, *J. Nanosci. Nanotechnol.*, 2018, **18**, 5390–5396.

28 P. Stolzenburg, A. Freytag, N. C. Bigall and G. Garnweitner, *CrystEngComm*, 2016, **18**, 8396–8405.

29 G. Bhanjana, N. Dilbaghi, S. Chaudhary, K. H. Kim and S. Kumar, *Analyst*, 2016, **141**, 4211–4218.

30 Z. Shu, X. Jiao and D. Chen, *CrystEngComm*, 2013, **15**, 4288–4294.

31 C. V. Reddy, B. Babu, I. N. Reddy and J. Shim, *Ceram. Int.*, 2018, **44**, 6940–6948.

32 R. Madhusudhana, M. A. Sangamesha, R. G. Krishne Urs, L. Krishnamurthy and G. L. Shekar, *Int. J. Adv. Res.*, 2014, **2**, 433–436.

33 H. S. Lim, A. Ahmad and H. Hamzah, *AIP Conf. Proc.*, 2013, **1571**, 812–816.

34 A. Bahari and M. Ghanbari, *Int. J. ChemTech Res.*, 2011, **3**, 1686–1691.

35 A. Majedi, F. Davar, A. Abbasi and A. Ashrafi, *J. Inorg. Organomet. Polym. Mater.*, 2016, **26**, 932–942.

36 G. Sponchia, E. Ambrosi, F. Rizzolio, M. Hadla, A. Del Tedesco, C. R. Spena, G. Toffoli, P. Riello and A. Benedetti, *J. Mater. Chem. B*, 2015, **3**, 7300–7306.

37 F. Davar and M. R. Loghman-Estarki, *Ceram. Int.*, 2014, **40**, 8427–8433.

38 M. Ramachandran, R. Subadevi, W. R. Liu and M. Sivakumar, *J. Nanosci. Nanotechnol.*, 2018, **18**, 368–373.

39 Y. T. Foo, A. Z. Abdullah, B. Amini Horri and B. Salamatinia, *Ceram. Int.*, 2019, **45**, 22930–22939.

40 H. J. Huang and M. C. Wang, *Ceram. Int.*, 2013, **39**, 1729–1739.

41 A. K. Singh and U. T. Nakate, *Sci. World J.*, 2014, 2014.

42 R. Dwivedi, A. Maurya, A. Verma, R. Prasad and K. S. Bartwal, *J. Alloys Compd.*, 2011, **509**, 6848–6851.

43 S. Baby Asha, D. Muthuraj, E. Kumar and V. Veeraputhiran, *J. Nanosci. Nanotechnol.*, 2019, **5**, 642–644.

44 S. Manjunatha and M. S. Dharmaprakash, *J. Lumin.*, 2016, **180**, 20–24.

45 M. R. H. Siddiqui, A. I. Al-Wassil, A. M. Al-Otaibi and R. M. Mahfouz, *Mater. Res.*, 2012, **15**, 986–989.

46 D. Prakash babu, R. Hari Krishna, B. M. Nagabhushana, H. Nagabhushana, C. Shivakumara, R. P. S. Chakradar, H. B. Ramalingam, S. C. Sharma and R. Chandramohan, *Spectrochim. Acta, Part A*, 2014, **122**, 216–222.

47 S. Tang, X. Huang, X. Chen and N. Zheng, *Adv. Funct. Mater.*, 2010, **20**, 2442–2447.

48 F. Davar, A. Hassankhani and M. R. Loghman-Estarki, *Ceram. Int.*, 2013, **39**, 2933–2941.

49 S. Iravani, H. Korbekandi, S. V. Mirmohammadi and B. Zolfaghari, *Res. Pharm. Sci.*, 2014, **9**, 385–406.

50 R. K. Das, V. L. Pachapur, L. Lonappan, M. Naghdi, R. Pulicharla, S. Maiti, M. Cledon, L. M. A. Dalila, S. J. Sarma and S. K. Brar, *Nanotechnol. Environ. Eng.*, 2017, **2**, 1–21.

51 K. N. Thakkar, S. S. Mhatre and R. Y. Parikh, *Nanomedicine*, 2010, **6**, 257–262.

52 N. I. Hulkoti and T. C. Taranath, *Colloids Surf., B*, 2014, **121**, 474–483.

53 T. Ahmed, H. Ren, M. Noman, M. Shahid, M. Liu, M. A. Ali, J. Zhang, Y. Tian, X. Qi and B. Li, *NanoImpact*, 2021, **21**, 100281.

54 I. Uddin and A. Ahmad, *J. Mater. Environ. Sci.*, 2016, **7**, 3068–3075.

55 V. Bansal, D. Rautaray, A. Ahmad and M. Sastry, *J. Mater. Chem.*, 2004, **14**, 3303–3305.

56 S. P. Suriyaraj, G. Ramadoss, K. Chandraraj and R. Selvakumar, *Mater. Sci. Eng., C*, 2019, **105**, 110021.

57 A. F. V. da Silva, A. P. Fagundes, D. L. P. Macuvele, E. F. U. de Carvalho, M. Durazzo, N. Padoin, C. Soares and H. G. Riella, *Colloids Surf., A*, 2019, **583**, 123915.

58 T. Van Tran, D. T. C. Nguyen, P. S. Kumar, A. T. M. Din, A. A. Jalil and D. V. N. Vo, *Environ. Chem. Lett.*, 2022, **20**, 1309–1331.

59 R. D. Abdul Jalill, M. M. H. M. Jawad and A. N. Abd, *J. Genet. Environ. Resour. Conserv.*, 2017, **5**, 6–23.

60 S. Shanthi and S. Sri Nisha Tharani, *Int. J. Eng. Appl. Sci.*, 2016, **3**, 257689.

61 P. Nimare and A. A. Koser, *Int. J. Eng. Technol.*, 2016, **3**, 1910–1912.

62 M. Sathishkumar, K. Sneha and Y. S. Yun, *Mater. Lett.*, 2013, **98**, 242–245.

63 S. Gowri, R. R. Gandhi and M. Sundrarajan, *J. Mater. Sci. Technol.*, 2014, **30**(8), 782–790.

64 A. Majedi, A. Abbasi and F. Davar, *J. Sol-Gel Sci. Technol.*, 2016, **77**, 542–552.

65 V. S. Saraswathi and K. Santhakumar, *J. Photochem. Photobiol., B*, 2017, **169**, 47–55.

66 B. Debnath, M. Majumdar, M. Bhowmik, K. L. Bhowmik, A. Debnath and D. N. Roy, *J. Environ. Manage.*, 2020, **261**, 110235.

67 S. Gowri, R. Rajiv Gandhi and M. Sundrarajan, *J. Mater. Sci. Technol.*, 2014, **30**, 782–790.

68 S. Balaji, B. K. Mandal, S. Ranjan, N. Dasgupta and R. Chidambaram, *J. Photochem. Photobiol., B*, 2017, **170**, 125–133.

69 A. Majedi, A. Abbasi and F. Davar, *J. Sol-Gel Sci. Technol.*, 2016, **77**, 542–552.

70 W. N. N. Wan Omar and N. A. S. Amin, *Fuel Process. Technol.*, 2011, **92**, 2397–2405.

71 F. Qiu, Y. Li, D. Yang, X. Li and P. Sun, *Bioresour. Technol.*, 2011, **102**, 4150–4156.

72 S. K. Das and S. A. El-Safty, *ChemCatChem*, 2013, **5**, 3050–3059.

73 Y. Zhang, W. T. Wong and K. F. Yung, *Appl. Energy*, 2014, **116**, 191–198.

74 M. Takase, M. Zhang, W. Feng, Y. Chen, T. Zhao, S. J. Cobbina, L. Yang and X. Wu, *Energy Convers. Manage.*, 2014, **80**, 117–125.

75 P. Patil and A. Pratap, *J. Oleo Sci.*, 2016, **65**, 331–337.

76 V. K. Booramurthy, R. Kasimani, S. Pandian and B. Ragunathan, *Environ. Sci. Pollut. Res.*, 2020, **27**, 20598–20605.

77 Y. F. Lin, J. H. Chen, S. H. Hsu, H. C. Hsiao, T. W. Chung and K. L. Tung, *J. Colloid Interface Sci.*, 2012, **368**, 660–662.

78 S. Gopinath, P. S. M. Kumar, K. A. Y. Arafath, K. V. Thiruvengadaravi, S. Sivanesan and P. Baskaralingam, *Fuel*, 2017, **203**, 488–500.

79 Y. Luo, Z. Mei, N. Liu, H. Wang, C. Han and S. He, *Catal. Today*, 2017, **298**, 99–108.

80 G. L. Shi, F. Yu, X. L. Yan and R. F. Li, *J. Fuel Chem. Technol.*, 2017, **45**, 311–316.

81 S. Dehghani and M. Haghighi, *Ultrason. Sonochem.*, 2017, **35**, 142–151.

82 I. Fatimah, D. Rubiyanto, A. Taushiyah, F. B. Najah, U. Azmi and Y. L. Sim, *Sustainable Chem. Pharm.*, 2019, **12**, 100129.

83 N. J. A. Rahman, A. Ramli, K. Jumbri and Y. Uemura, *Sci. Rep.*, 2019, **9**, 1–12.

84 J. H. Cavka, S. Jakobsen, U. Olsbye, N. Guillou, C. Lamberti, S. Bordiga and K. P. Lillerud, *J. Am. Chem. Soc.*, 2008, **130**, 13850–13851.

85 M. Kandiah, M. H. Nilsen, S. Usseglio, S. Jakobsen, U. Olsbye, M. Tilset, C. Larabi, E. A. Quadrelli, F. Bonino and K. P. Lillerud, *Chem. Mater.*, 2010, **22**, 6632–6640.

86 J. B. Decoste, G. W. Peterson, H. Jasuja, T. G. Glover, Y. G. Huang and K. S. Walton, *J. Mater. Chem. A*, 2013, **1**, 5642–5650.

87 X. Liu, N. K. Demir, Z. Wu and K. Li, *J. Am. Chem. Soc.*, 2015, **137**, 6999–7002.

88 L. Valenzano, B. Civalleri, S. Chavan, S. Bordiga, M. H. Nilsen, S. Jakobsen, K. P. Lillerud and C. Lamberti, *Chem. Mater.*, 2011, **23**, 1700–1718.

89 A. Schaate, P. Roy, A. Godt, J. Lippke, F. Waltz, M. Wiebcke and P. Behrens, *Chem.–Eur. J.*, 2011, **17**, 6643–6651.

90 F. Zhou, N. Lu, B. Fan, H. Wang and R. Li, *J. Energy Chem.*, 2016, **25**, 874–879.

91 A. S. Abou-Elyazed, G. Ye, Y. Sun and A. M. El-Nahas, *Ind. Eng. Chem. Res.*, 2019, **58**, 21961–21971.

92 W. Xie and F. Wan, *Chem. Eng. J.*, 2019, **365**, 40–50.

93 N. Lu, X. Zhang, X. Yan, D. Pan, B. Fan and R. Li, *CrystEngComm*, 2019, **22**, 44–51.

94 Q. Zhang, D. Lei, Q. Luo, J. Wang, T. Deng, Y. Zhang and P. Ma, *RSC Adv.*, 2020, **10**, 8766–8772.

95 Y. Zhou, I. Noshadi, H. Ding, J. Liu, R. S. Parnas, A. Clearfield, M. Xiao, Y. Meng and L. Sun, *Catalysts*, 2018, **8**(1), 17.

96 S. Zinatloo-Ajabshir and M. Salavati-Niasari, *J. Mol. Liq.*, 2016, **216**, 545–551.

97 J. Zhang, Y. Gao, X. Jia, J. Wang, Z. Chen and Y. Xu, *Sol. Energy Mater. Sol. Cells*, 2018, **182**, 113–120.

98 S. N. Basahel, T. T. Ali, M. Mokhtar and K. Narasimharao, *Nanoscale Res. Lett.*, 2015, **10**(1), 1–13.

99 N. Al-Zaqri, A. Muthuvel, M. Jothibas, A. Alsalme, F. A. Alharthi and V. Mohana, *Inorg. Chem. Commun.*, 2021, **127**, 108507.

100 H. M. Shinde, T. T. Bhosale, N. L. Gavade, S. B. Babar, R. J. Kamble, B. S. Shirke and K. M. Garadkar, *J. Mater. Sci.: Mater. Electron.*, 2018, **29**, 14055–14064.

101 S. Haq, H. Afsar, I. U. Din, P. Ahmad, M. U. Khandaker, H. Osman, S. Alamri, M. I. Shahzad, N. Shahzad, W. Rehman and M. Waseem, *Catalysts*, 2021, **11**(12), 1481.

102 K. Gurushantha, K. S. Anantharaju, L. Renuka, S. C. Sharma, H. P. Nagaswarupa, S. C. Prashantha, Y. S. Vidya and H. Nagabhushana, *RSC Adv.*, 2017, **7**, 12690–12703.

103 P. Rasheed, S. Haq, M. Waseem, S. U. Rehman, W. Rehman, N. Bibi and S. A. A. Shah, *Mater. Res. Express*, 2020, **7**(2), 025011.

104 M. Imran, S. Riaz, I. Sanaullah, U. Khan, A. N. Sabri and S. Naseem, *Ceram. Int.*, 2019, **45**, 10106–10113.

105 M. Kumaresan, K. Vijai Anand, K. Govindaraju, S. Tamilselvan and V. Ganesh Kumar, *Microb. Pathog.*, 2018, **124**, 311–315.

106 F. C. P. Masim, C. H. Tsai, Y. F. Lin, M. L. Fu, M. Liu, F. Kang and Y. F. Wang, *Environ. Technol.*, 2019, **40**, 226–238.

107 J. B. Fathima, A. Pugazhendhi and R. Venis, *Microb. Pathog.*, 2017, **110**, 245–251.

108 A. Precious Ayanwale and S. Y. Reyes-López, *ACS Omega*, 2019, **4**, 19216–19224.

109 M. Khan, M. R. Shaik, S. T. Khan, S. F. Adil, M. Kuniyil, M. Khan, A. A. Al-Warthan, M. R. H. Siddiqui and M. Nawaz Tahir, *ACS Omega*, 2020, **5**, 1987–1996.

110 A. Derbalah, M. M. Elsharkawy, A. Hamza and A. El-Shaer, *Pestic. Biochem. Physiol.*, 2019, **157**, 230–236.

111 L. Chen, H. Zhong, X. Qi, H. Shao and K. Xu, *RSC Adv.*, 2019, **9**, 13220–13233.

112 C. Han, J. Yang and J. Gu, *J. Nanopart. Res.*, 2018, **20**(3), 1–11.

113 F. M. Alzahrani, K. M. S. Katubi, D. Ali and S. Alarifi, *Int. J. Nanomed.*, 2019, **14**, 7003–7016.

114 A. Mftah, F. H. Alhassan, M. S. Al-Qubaisi, M. E. El Zowalaty, T. J. Webster, M. Sh-Eldin, A. Rasedee, Y. H. Taufiq-Yap and S. S. Rashid, *Int. J. Nanomed.*, 2015, **10**, 765–774.

115 A. Ghosh, S. Kanrar, P. Nandi, P. Sasikumar, K. Biswas and U. C. Ghosh, *J. Chem. Eng. Data*, 2020, **65**, 885–895.

116 Y. Sun, M. Chen, H. Liu, Y. Zhu, D. Wang and M. Yan, *Appl. Surf. Sci.*, 2020, **525**, 146614.

117 R. Bhatt, V. Ageetha, S. B. Rathod and P. Padmaja, *Carbohydr. Polym.*, 2019, **208**, 441–450.

118 S. Salehi, S. Alijani and M. Anbia, *Int. J. Biol. Macromol.*, 2020, **164**, 105–120.

119 J. Wang, X. Shao, J. Liu, Q. Zhang, J. Ma and G. Tian, *Mater. Chem. Phys.*, 2020, **249**, 123024.

120 X. Fang, S. Wu, Y. Wu, W. Yang, Y. Li, J. He, P. Hong, M. Nie, C. Xie, Z. Wu, K. Zhang, L. Kong and J. Liu, *Appl. Surf. Sci.*, 2020, **518**, 146226.

121 K. Shehzad, M. Ahmad, C. Xie, D. Zhan, W. Wang, Z. Li, W. Xu and J. Liu, *J. Hazard. Mater.*, 2019, **373**, 75–84.

122 A. Hafezeqoran and R. Koodaryan, *BioMed Res. Int.*, 2017, **2017**, 9246721.

123 M. Aivazi, M. Fathi, F. Nejatidanesh, V. Mortazavi, B. H. Beni and J. P. Matinlinna, *J. Lasers Med. Sci.*, 2018, **9**, 87–91.

124 T. Tahsili, W. Park, M. Hirota, N. M. Rezaei, M. Hasegawa, M. Ishijima, K. Nakhaei, T. Okubo, T. Taniyama,

A. Ghassemi, T. Tahsili, W. Park, M. Hirota and T. Ogawa, *Int. J. Nanomed.*, 2018, **13**, 3381–3395.

125 P. Yu, C. Wang, J. Zhou, L. Jiang, J. Xue and W. Li, *BioMed Res. Int.*, 2016, **2016**, 8901253.

126 M. M. Gad, R. Abualsaud, A. Rahoma, A. M. Al-Thobity, K. S. Al-Abidi and S. Akhtar, *Int. J. Nanomed.*, 2018, **13**, 283–292.

127 U. Lohbauer, A. Wagner, R. Belli, C. Stoetzel, A. Hilpert, H. D. Kurland, J. Grabow and F. A. Müller, *Acta Biomater.*, 2010, **6**, 4539–4546.

128 M. M. Gad, A. M. Al-Thobity, S. Y. Shahin, B. T. Alsaqer and A. A. Ali, *Int. J. Nanomed.*, 2017, **12**, 5409–5419.

129 Y. Oshima, F. Iwasa, K. Tachi and K. Baba, *Int. J. Oral. Maxillofac. Implants*, 2017, **32**, 81–91.

130 R. Yamada, K. Nozaki, N. Horiuchi, R. Nemoto, H. Miura and A. Nagai, *Mater. Sci. Eng., C*, 2017, **78**, 1054–1060.

131 Z. Zhang, C. Zhang and X. Zhang, *Analyst*, 2002, **127**, 792–796.

132 K. M. Garadkar, B. S. Shirke, Y. B. Patil, D. R. Patil, *Sensors and transducers*, 2009, Vol. 110, Iss. 11, pp. 17–25.

133 C. O. Chikere, N. H. Faisal, P. Kong-Thoo-Lin and C. Fernandez, *Nanomaterials*, 2020, **10**(3), 537.

134 J. Wang, M. Y. Su, J. Q. Qi and L. Q. Chang, *Sens. Actuators, B*, 2009, **139**, 418–424.

135 J. Gong, X. Miao, H. Wan and D. Song, *Sens. Actuators, B*, 2012, **162**, 341–347.

136 T. Trinadh, H. Khuntia, T. Anusha, K. S. Bhavani, J. V. S. Kumar and P. K. Brahman, *Diamond Relat. Mater.*, 2020, **110**, 108143.

137 J. Der Liao, K. Sivashanmugan, B. H. Liu, W. E. Fu, C. C. Chen, G. D. Chen and Y. Der Juang, *Nanomaterials*, 2018, **8**(6), 402.

138 C. Yu, G. Liu, B. Zuo and R. Tang, *Luminescence*, 2009, **24**, 282–289.

139 A. V. Borhade, D. R. Tope and J. A. Agashe, *J. Mater. Sci.: Mater. Electron.*, 2018, **29**, 7551–7561.

140 R. Jain, D. C. Tiwari and S. Shrivastava, *J. Electrochem. Soc.*, 2014, **161**, B39–B44.

141 T. N. Myasoedova, T. S. Mikhailova, G. E. Yalovega and N. K. Plugotarenko, *Chemosensors*, 2018, **6**(4), 67.

142 F. Maleki and G. Pacchioni, *Top. Catal.*, 2020, **63**, 1717–1730.

143 A. R. Puigdollers, F. Illas and G. Pacchioni, *J. Phys. Chem. C*, 2016, **120**, 4392–4402.

144 L. Liu, X. Su, H. Zhang, N. Gao, F. Xue, Y. Ma, Z. Jiang and T. Fang, *Appl. Surf. Sci.*, 2020, **528**, 146900.

145 A. Ruiz Puigdollers, F. Illas and G. Pacchioni, *Rend. Lincei.*, 2017, **28**, 19–27.

146 N. Kumari, M. K. Aulakh, S. Sareen, A. Sharma, H. S. Sohal, M. Verma, S. K. Mehta and V. Mutreja, *Top. Catal.*, 2022, DOI: **10.1007/s11244-022-01652-z**.